JOURNAL OF GEOPHYSICAL RESEARCH, VOL. 96, NO. C5, PAGES 8643–8663, MAY 15, 1991

Concurrent High Resolution Bio-optical and Physical Time Series Observations in the Sargasso Sea During the Spring of 1987

T. DICKEY,[1] J. MARRA,[2] T. GRANATA,[1] C. LANGDON,[2] M. HAMILTON,[1] J. WIGGERT,[1] D. SIEGEL[1,3] AND A. BRATKOVICH[1,4]

The evolution of bio-optical and physical properties of the upper layer of the open ocean has been examined at time scales from a few minutes to several months using recently developed multi-variable moored systems (MVMS). Concurrent, colocated time series measurements of horizontal currents, temperature, photosynthetically available radiation, transmission of a beam of collimated light (660 nm), stimulated chlorophyll fluorescence, and dissolved oxygen concentration were made. The systems were located at eight depths in the upper 160 m of the Sargasso Sea (34°N, 70°W) and were deployed three times for a total of 9 months in 1987. The first deployment data presented here show considerably more variability than those of the latter two deployments because of the dynamic springtime shoaling of the mixed layer and the accompanying phytoplankton bloom and more mesoscale variability associated with cold core rings and warm outbreak waters associated with the Gulf Stream. These data are used to demonstrate the utility of the MVMS and indicate the importance of high-frequency, long-term sampling of bio-optical and physical variables of the upper ocean for understanding and modeling dynamical changes in bio-optical properties, primary production, and carbon fluxes of the upper ocean on time scales ranging from minutes to seasons to decades. Some phenomena observed with the systems include (1) diurnal variations in bio-optical properties, (2) springtime stratification and rapid (~2 days and less) episodic changes in the beam attenuation coefficient and in situ chlorophyll fluorescence, and (3) advective episodes associated with warm outbreaks of Gulf Stream waters and cold core Gulf Stream rings in the vicinity of the mooring.

1. INTRODUCTION

The understanding of the ecology of the upper ocean and its temporal and spatial variability requires interdisciplinary measurements. The present study was a major component of the Office of Naval Research sponsored Biowatt program and concerns the ecology of the upper ocean planktonic community. The Biowatt program was motivated in part by the desire to improve our understanding of the variability of upper ocean bio-optical properties as affected by physical forcing. A simple conceptual model may be used to illustrate some of the important aspects of this problem. The structure of the upper ocean is regulated by the fluxes of momentum, heat, and light from the atmosphere. These fluxes affect temporal and spatial changes in distributions of plant nutrients, phytoplankton, zooplankton, and other biogenic matter, all of which can contribute to bio-optical variations. Advection and a variety of biological processes (e.g., predation, phytoplankton light adaptation, nutrient cycling, etc.) are important as well.

One of the objectives of Biowatt was to obtain measurements to enable the determination of cyclic (e.g., diurnal, tidal, seasonal, etc.) and episodic (e.g., synoptic weather event scale, advective transport of materials, phytoplankton blooms, etc.) changes in the physical, optical, and biological environment [*Dickey et al.*, 1986*a*]. It was hypothesized that these measurements were required to identify key processes, to establish statistical relationships among fundamentally related physical and bio-optical parameters, and ultimately to model production rates of the upper ocean

Within the past decade, several in situ and remote sensing systems relevant to the physics, bio-optics, and ecology of the upper ocean have been developed and deployed. The advantages and disadvantages of various platforms and their relevant spatial and temporal sampling ranges and resolutions have been reviewed recently by *Dickey* [1988, 1990, 1991]. Only within the past few years have upper ocean physical experiments been successfully conducted for periods of more than a few months and with temporal resolution of the order of minutes [e.g., *Briscoe and Weller*, 1984]. This was due to cruise length constraints as well as the difficulties involved with upper ocean instrumentation. The biological, as well as physical, dynamics of the pelagic ocean are highly intermittent [e.g., *Platt et al.*, 1989]; yet time series observations relevant to bio-optical processes and primary productivity have been either coarse in temporal resolution (e.g., biweekly [*Menzel and Ryther*, 1960, 1961]), short in duration (e.g., typically a maximum of a few weeks [*Whitledge and Wirick*, 1983, 1986; *Dickey et al.*, 1986*b*; *Thomson et al.*, 1988; *Siegel et al.*, 1989; *Washburn et al.*, 1989] or done in coastal waters [e.g., *Cullen et al.*, 1983; *Whitledge and Wirick*, 1983, 1986; *Booth et al.*, 1987; *Falkowski et al.*, 1988; *Thomson et al.*, 1988; *Fukuchi et al.*, 1988, 1989] or lakes [e.g., *Powell et al.*, 1975]. The observations reported here and those presented in a companion paper by *Smith et al.* [this issue] are the first long-term, high-resolution time series measurements of bio-optical and physical variables in the open ocean.

Since many of the important energetic physical and bio-optical processes have time scales ranging from minutes to hours, aliasing is a serious problem for sampling done with coarse temporal resolution. For example, episodic events often occur intermittently on intervals of days to several weeks. Thus in order to obtain statistically significant data capable of resolving this broad range of variability scales, sampling must be done rapidly (to satisfy the Nyquist sampling theorem) and over periods of several months in order to observe environmentally significant events.

[1]Ocean Physics Group, Department of Geological Sciences, University of Southern California, Los Angeles.

[2]Lamont-Doherty Geological Observatory, Palisades, New York.

[3]Now at Department of Geography, University of California, Santa Barbara, Santa Barbara.

[4]Now at NOAA Great Lakes Environmental Research Laboratory, Ann Arbor, Michigan, and Department of Atmospheric, Oceanic, and Space Sciences, University of Michigan, Ann Arbor.

Paper number 91JC00413.
0148-0227/91/91JC-00413$05.00

These sampling considerations were critical to the development of a new system, the multi-variable moored system (MVMS). The MVMS is capable of obtaining a set of concurrent, colocated physical and bio-optical measurements at a high sampling rate (every 4 min) for a period of several months. It is noteworthy that the Nyquist period for the present study is 8 min, a significant improvement over the Nyquist period of 1 month which was applicable to the pioneering studies by *Menzel and Ryther* [1960, 1961] in the Sargasso Sea. The MVMS provides physical and bio-optical data amenable to various spectral analysis techniques, which may be used to determine significant time scales, correlations, phases, and spectral energy power laws. Ultimately, these data may be used to identify critical processes and feedback mechanisms [e.g., *Musgrave et al.*, 1988], statistically quantify relationships, and formulate and test coupled bio-optical and physical models.

Data obtained from the MVMS may also be used for estimating particulate pigment biomass from beam attenuation [e.g., *Bishop*, 1986; *Siegel et al.*, 1989] and stimulated chlorophyll fluorescence data [e.g., *Welschmeyer and Lorenzen*, 1986], for primary productivity determinations using beam attenuation [e.g., *Siegel et al.*, 1989], dissolved oxygen [e.g., *Emerson*, 1987], and stimulated fluorescence data [e.g., *Kiefer and Mitchell*, 1983; *Welschmeyer and Lorenzen*, 1986], and for estimating the vertical flux of particulate carbon from the euphotic layer [e.g., *Eppley and Peterson*, 1979; *Jenkins and Goldman*, 1985; *Dickey*, 1991]. Estimates of pigment biomass and primary productivity using data obtained from the MVMS and the bio-optical moored system (BOMS) [see *Smith et al.*, this issue] can be intercompared and used for examining variations in the attenuation of solar radiation due to distributions of pigment concentration [e.g., *Siegel and Dickey*, 1987]. Determining and modeling primary productivity and carbon flux are of considerable interest in the context of global biogeochemical fluxes across the air-sea interface and through the interior of the ocean as they relate to the global carbon budget [e.g., *Brewer et al.*, 1986]. The moored systems described here can be used to provide relevant bio-optical and physical information on time scales unachievable from sampling by ship, airplane, or satellite platforms and depth scales unobtainable from the latter two platform types. These systems can be particularly useful for providing complementary data for remotely sensed observations [*e.g., Smith et al.*, 1987*a, b*; *Michaelsen et al.*, 1988; *Dickey*, 1988, 1990, 1991] and for studies employing a variety of sampling platforms which provide horizontal spatial information.

The purpose of this report is to (1) describe the MVMS, (2) present observations obtained in the Sargasso Sea during the late winter to mid-springtime deployment period, and (3) provide a preliminary interpretation of some of the MVMS data. Early results emphasizing the bio-optical variability and diurnal cycles of bio-optical properties and dissolved oxygen have been presented by *Dickey et al.* [1990*a,b*] and *Hamilton et al.* [1990], respectively. The complete data set (full 9 months) and other specific topics (e.g., primary production, carbon fluxes, dissolved oxygen variability, etc.) will be addressed in forthcoming papers.

2. METHODS

The Biowatt mooring was located in the open ocean waters (depth ~5400 m) of the Sargasso Sea (34°N, 70°W; Figure 1). Moorings were deployed at the site in 1987 during three periods (February 28 to May 11, May 13 to August 30, and August 31 to November 23) and thus spanned the oceanic seasons. Only the first deployment observations (70 days) are discussed here.

The basic development philosophy for the system was to utilize state-of-the-art sensors and a data acquisition system that had been well tested and successfully deployed in the field and to measure key physical and bio-optical variables at a high sampling frequency. A schematic of the MVMS and the Biowatt mooring is shown in Figure 2. The sensor suite for the system includes: a vector measuring current meter (VMCM) for horizontal velocity measurements [*Weller and Davis*, 1980], a thermistor for temperature measurements, a conductivity sensor (on 14 m and 160

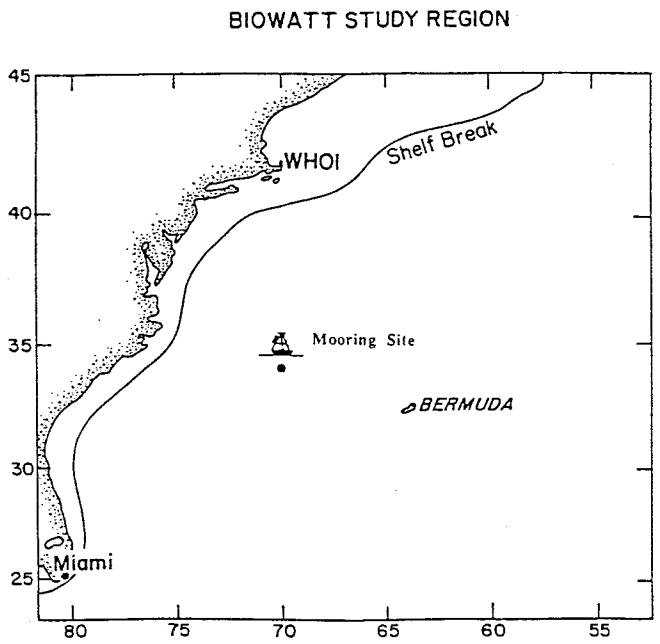

Fig. 1. Location of the Biowatt mooring for the 1987 field study.

m MVMS's only), a beam transmissometer [*Bartz et al.*, 1978], a strobe in situ fluorometer [*Bartz et al.*, 1988], a photosynthetically available radiation (PAR) sensor [*Booth*, 1976], and a pulsed electrode dissolved oxygen sensor [*Langdon*, 1984]. Antifoulants were applied to to the various components of the system. A clear antifoulant OMP-8, which is an organo-metallo-polymer, was applied to the optical sensors, and Aquatek was used for the dissolved oxygen electrodes. The advantages and disadvantages of application of OMP-8 to the transmissometer windows are discussed by *Spinrad* [1987]. Our results suggest that the antifoulants were effective with minimal degradation of data because of biofouling effects.

Data were taken every 4 min and consisted of 4 min averages for all sensors except the fluorometer and the dissolved oxygen sensor, which were sampled instantaneously. Standard laboratory calibrations were done for thermistors and conductivity sensors, although the conductivity measurements did not turn out to be useful for the interpretation of the data because of the dynamic range. The beam transmissometers (25 cm path length) measure the extinction of a beam of 660 nm light as attenuated (scattered) primarily by particles ranging in diameter from approximately ~1 μm to 80 μm [*Spinrad*, 1986]. They were calibrated in air with the path blocked and free of obstruction. PAR sensors measure quantum scalar irradiance in the waveband 400 - 700 nm. The PAR sensors and current meters were calibrated by the manufacturers. The fluorometers were calibrated in the laboratory using a phytoplankton culture of *Thalassiosira pseudonana*, a centric diatom, and the fluorescence signal is well correlated with chlorophyll-*a*. The various errors associated with this measurement are estimated to total between 10 and 20% (J. Marra and C. Langdon, An evaluation of in situ fluorometers for the estimation of chlorophyll *a*, submitted to *Mar. Ecol. Prog. Ser.*, 1990). It should be noted that there is additional uncertainty in the reported field measurements of chlorophyll-*a* because of variations in the chlorophyll to fluorescence ratio which are caused by several factors including (1) phytoplankton species reported at the site for the springtime period [*Bidigare et al.*, 1989] and (2) light and nutrient stresses [e.g., *Kiefer*, 1973]. These associated errors are difficult to quantify, but could be quite significant. Details concerning the MVMS sensors and their calibrations are given by *Dickey et al.* [1990*a*].

Meteorological sensors mounted on a surface buoy measured atmospheric pressure, wind speed and direction, air and near surface sea temperatures, relative humidity, and shortwave solar radiation

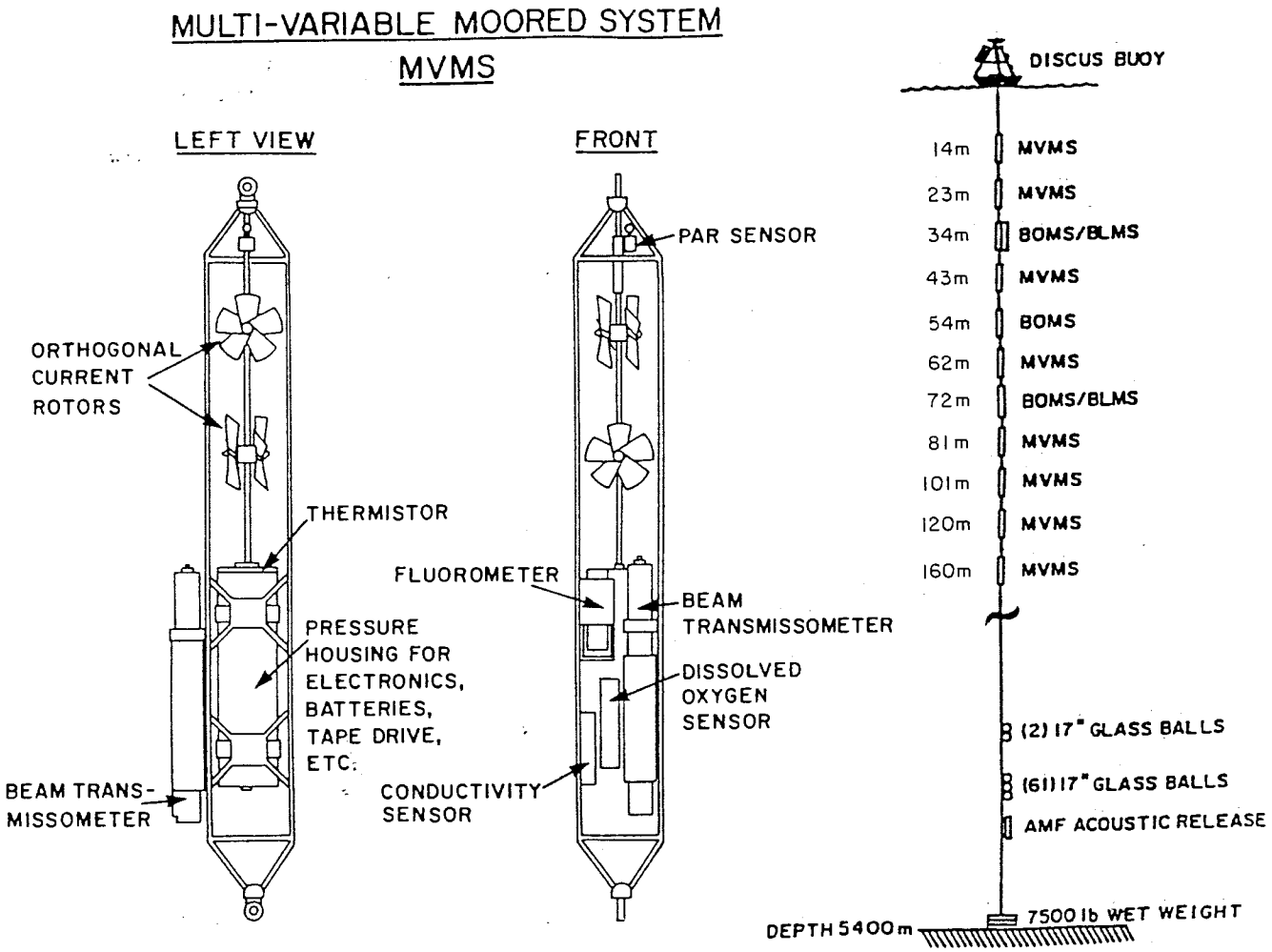

Fig. 2. Diagrams illustrating the multi-variable moored system (MVMS) with its various sensors and the Biowatt mooring configuration including the depths of the MVMS, BOMS, and BLMS systems.

[*Dean and Beardsley*, 1988; *Weller et al.*, 1990]. The meteorological data (using 7.5 min averages) were used to determine the fluxes of momentum, heat, and light across the air-water interface. Wind stress and heat fluxes were computed using the procedures of *Liu et al.* [1984] and the drag coefficients of *Kondo* [1975] using the algorithms provided by *Liu and Blanc* [1984].

The subsurface moored instrument array for the first deployment period included eight MVMS units at nominal depths of 14, 23, 43, 62, 81, 101, 120, and 160 m, BOMS [*Booth and Smith*, 1988; *Smith et al.*, this issue] at 33 and 52 m, and bioluminescence moored systems or BLMS [*Swift et al.*, 1988] at 33 and 52 m. The depth estimates are based on mooring component lengths and some variability (few meters) results from changing current structure. There are no MVMS data from 120 m because of a data tape failure. The mooring configuration and instrument depths are shown in Figure 2. The BOMS collected downwelling irradiance (wavelengths of 410, 441, 488, 520, and 560 nm), upwelling radiance (wavelengths of 410, 441, 488, 520, and 683 nm), temperature, pressure, and tilt data. Shipboard bio-optical and conductivity-temperature-depth (CTD) profile data were collected in the vicinity of the mooring near the times of instrument deployment and recovery [*Smith et al.*, this issue; Marra and Langdon, 1990].

Broadband data are not presented here for the sake of brevity. Data in all figures have been band passed by convolving the data using a Gaussian window (either 2 or 24 hours). This method was selected because of its excellent frequency response characteristics and minimal aliasing effect. The autospectra of several physical and bio-optical variables have been determined (Figures 11a through 11f) using standard signal processing techniques. The data records for each variable were divided into overlapping ensembles of 8192 points (corresponding to 22.76 days) which increased the confidence of the spectral estimates while still allowing examination of lower-frequency (i.e., mesoscale) events. In addition, the spectra were smoothed at frequencies greater than the semidiurnal frequency using band averaging. The diurnal (D), semidiurnal (SD), and local inertial (I) frequencies have been indicated. The two components of the current and wind data represent a vector time series and have been combined and then resolved into clockwise (CW) and counterclockwise (CCW) components [*e.g., Gonella*, 1972].

3. OBSERVATIONS

The present observations were made at the LOTUS (Long-Term Upper-Ocean Study) site (34°N, 70°W; see Figure 1), which was selected because of its geographic accessibility, the availability of historical and recent physical [e.g., *Bunker*, 1975, 1976; *Hellerman and Rosenstein*, 1983; *Richardson*, 1983; *Briscoe and Weller*, 1984; *Dickey et al.*, 1986c] and bio-optical [*e.g., Menzel and Ryther*, 1960, 1961; *Brown et al.*, 1985; *Bidigare et al.*, 1989; *Marra et al.*, 1990; *Siegel et al.*, 1990] data in the general vicinity of the site. The selection of the site was also motivated by the desire to observe intermittent and seasonal changes (e.g., wind events, the spring bloom of phytoplankton, etc.), identified as energetic components in the historical data bases.

The Sargasso Sea is characterized by a variety of oceanic and atmospheric conditions. Among these are (1) the daily and seasonal heating cycle, (2) episodic wind forcing associated with frontal passages and on occasion hurricanes, (3) internal gravity waves and tides, (4) small-scale mixing events associated with atmospheric forcing and current shears, and (5) advectively forced variability such as cold core rings and warm water outbreaks associated with the Gulf Stream. The occurrences of the latter mesoscale features are of particular interest in the context of time series observations from a fixed mooring, since they are known sources of ecological variability.

To facilitate interpretation, the data were subdivided into six observational periods which were selected on the basis of either temperature structure, current regime, or bio-optical properties. Satellite images from the advanced very high resolution radiometer (AVHRR) and Geosat have been examined for detailed sea surface temperature and sea surface elevation structures [*Chai et al.*, 1991], respectively. In addition, representative sea surface temperature maps (for Julian days (JD) 68, 84, 96, 103, 114, and 121; Figure 3) for the general geographical region (provided by the NOAA Ocean Services Unit) have been selected for each of the periods. These maps facilitate the interpretation of the data in the context of horizontal features such as cold core rings and warm outbreaks of Gulf Stream waters which have been reported in the vicinity of the mooring site in the past [e.g., *Cornillon et al.*, 1986].

Temporal variability in wind stress and heat flux time series are shown in Figure 4. The winds are variable and episodes of relatively high winds (~15 m s^{-1} at 10 m height above the sea surface) are associated with synoptic scale weather systems (typically 2 - 5 days in duration). The incoming shortwave radiation, Q_{sw}, is modulated by clouds and increases as expected in the late winter to early springtime period. The latent heat flux, Q_{le}, dominates the heat loss terms, with the next most important term being the net longwave radiation Q_{lw}. The latent heat flux term can be 2 to 3 times as great as the longwave term during periods of calm weather. The mooring site is near the geographic location marked by the greatest annual heat loss to the atmosphere in the North Atlantic [*Bunker*, 1976]. The net heat flux exhibits a diurnal modulation and has a peak value of ~800 W m^{-2} and a maximum heat loss value of nearly 600 W m^{-2}. The daily mean net heat flux increases through the first deployment due to the seasonal cycle. The present meteorological data are consistent with the climatological data reported by *Bunker* [1976] and other data taken with sensors comparable to those used for the present experiment at the mooring site [*Deser et al.*, 1983].

The 2-hour filtered time series of temperature obtained from seven of the eight MVMS units are shown in Figure 5. This representation facilitates the interpretation of the data and provides a means of describing the context of several of the other measurements. Some of the primary phenomena readily discernible from the time series of temperature (Figure 5), mixed layer depth and 1% light level (Figure 6), currents (Figure 7), and bio-optical properties (Figures 8 and 9) include (1) the onset of springtime stratification and shoaling of the mixed layer, (2) mesoscale advective episodes and accompanying changes in bio-optical properties, (3) synoptic-scale changes forced by wind and cloud conditions, and (4) diurnal variations in the bio-optical variables.

The sequence of events for the six periods is summarized below. The general criteria described above are used to distinguish these periods.

Period 1: Julian Days 60-79, March 1 to 20, 1987

During the first period, the seasonal mixed layer is generally quite deep (>160 m) but warm outbreak waters derived from the Gulf Stream apparently advect through the mooring site. This is

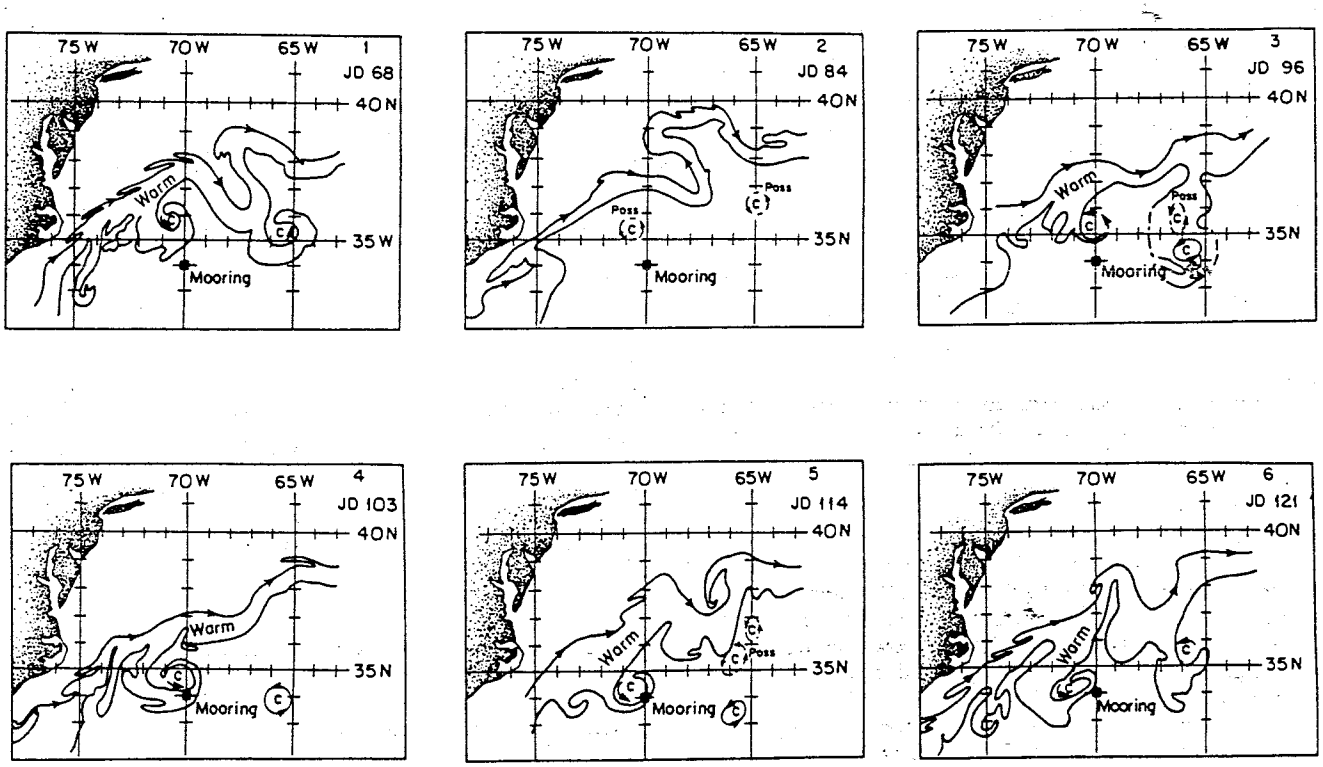

Fig. 3. The general region of the Biowatt study and the location of the Biowatt mooring. The path of the Gulf Stream, its associated warm outbreaks, and cold core rings as determined from sea surface temperature data are shown. Individual panels are shown to indicate the primary advective features representative of the six individual time periods (as indicated in Figure 4).

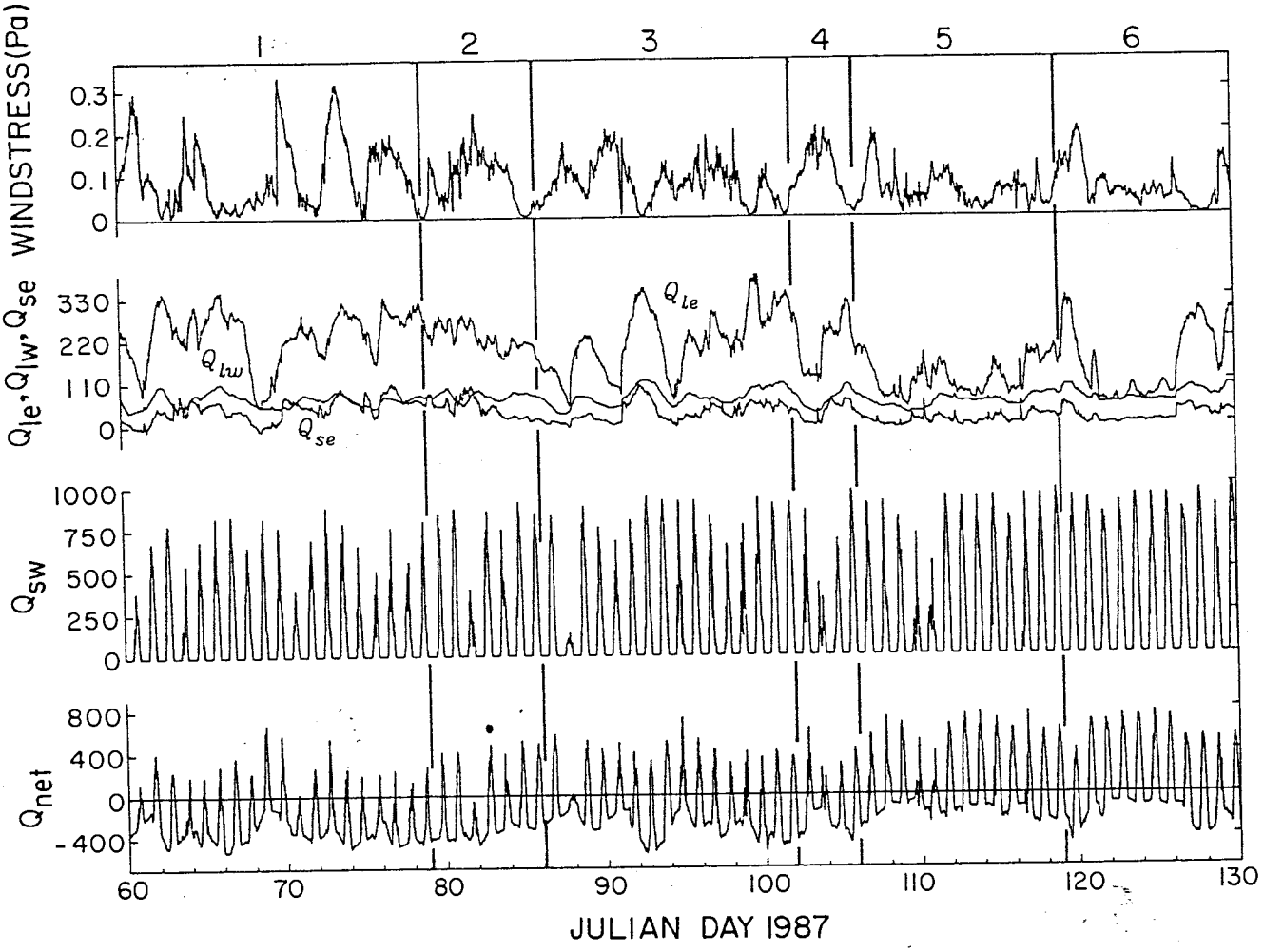

Fig. 4. Time series of wind stress in Pa, latent heat flux (Q_{le}), net longwave heat flux (Q_{lw}), sensible heat flux (Q_{se}), shortwave radiation (Q_{sw}), and net heat flux (Q_{net}). All heat fluxes are in W m^{-2}. The first deployment time series is subdivided into 6 periods in order to facilitate the discussion of the data set.

evidenced by the oscillation of the mixed layer depth and the isotherms within the upper 160 m (Figure 6). This interpretation is supported by the fact that the isothermal periods do not necessarily correspond to wind events. Also, short time scale variability is apparent in some of the bio-optical properties (Figure 8).

The meteorological conditions during the first period are marked by three wind events during which wind speeds are ~15 m s^{-1} (wind stress $\tau \sim 0.3$ Pa; Figure 4). These wind events and those observed throughout the experiment are generally correlated with the passage of significant low-pressure systems as indicated by the time series of the barometric pressure (not shown).

In the following, time series at fixed depths and time-depth contours of several physical and bio-optical variables are described. The first period is characterized by a high degree of variability in temperature with excursions in the near-surface layer greater than 1°C occurring on a nominal time scale of the order of a day. During the warm intervals, there is considerable stratification (of the order of 1°C/150 m); however the upper layer is nearly isothermal (~18.7°C) during the cold intervals. The daily mean mixed layer depth, which is defined as the depth at which the temperature difference from the surface value exceeds 0.1°C, correspondingly varies from ~25 m to greater than 160 m (Figure 6). The depth of the mixed layer is highly variable on a scale of a few days.

The extreme temperature and mixed layer depth variations are likely to be caused by warm outbreak waters originating from the Gulf Stream (Figure 3). *Cornillon et al.* [1986] describe warm outbreaks as large bodies of Gulf Stream water, which detach from the Gulf Stream and then exist as well-defined entities. They describe outbreak features which form within a few days, persist for ~10 - 20 days, and have dimensions of the order of 100 - 200 km. The sea surface temperature map for JD 68 appears to show such an outbreak to the northwest of the mooring site (Figure 3). The map is based on a compilation of data from a variety of sources (e.g., ships, satellite AVHRR, etc.) using 3-day averages. The exact location of the feature and its associated movement are not resolvable to the degree required for a strict interpretation. It is possible that the mooring may have been located at a position near a boundary between warm outbreak waters and Sargasso Sea waters and thus it may have sensed the differing waters (cooler Sargasso Sea water and warmer Gulf Stream outbreak water) as they meandered about the mooring site.

The currents are generally toward the south during this period with mean near-surface speeds of approximately 50 cm s^{-1} and a maximum value of ~125 cm s^{-1}. The time series of daily mean

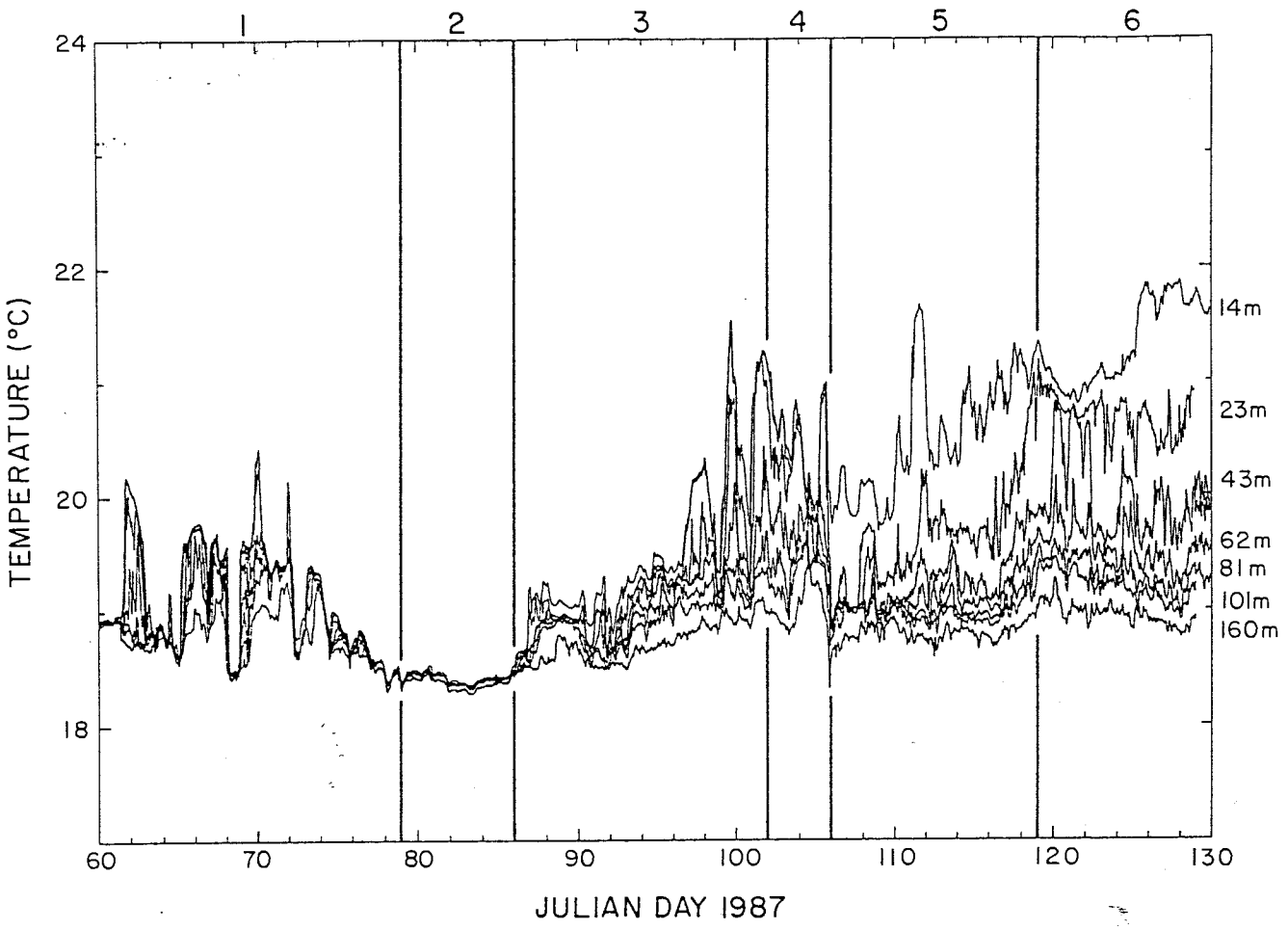

Fig. 5. Time series of temperature for 7 depths in the upper 160 m.

current velocities are shown in Figures 7*a* and 10*c*. There is a large amount of current variability in direction and magnitude. This variation might help to explain the temperature oscillations if the mooring were indeed near the water mass boundary hypothesized above. The kinetic energy (actually the squared magnitude of the horizontal speed) is nearly constant, though slightly decreasing, with depth. The currents are consistent with previous observations at the site by *Briscoe and Weller* [1984].

Shear is defined as

$$\text{Shear} = \sqrt{(\Delta u/\Delta z)^2 + (\Delta v/\Delta z)^2}$$

where u and v are the horizontal components of the currents and z is the depth coordinate. Shear time series show higher levels in the upper 60 m and episodic variations (Figure 7c). The near surface (upper 40 m) shear appears to be modulated by the wind events, whereas the deeper shear (greater than 40 m) seems to be more related to stratification changes (Figures 10*b* and 10*d*).

The rotary spectra of horizontal currents for the first deployment period indicate that there is considerable energy in the frequency bands encompassing the diurnal, semidiurnal, and inertial (21.5 hour) periods (Figures 11*b* and 11*c*, for depths of 23 and 101 m). There also appears to be considerable energy at subinertial frequencies. This energy is probably related to energetic advective episodes associated with warm outbreaks and a cold core ring in the vicinity of the mooring. There is a greater contribution by the clockwise opposed to the counterclockwise component for the upper water column (Figure 11*b*) near the inertial frequency as expected. This effect is reduced for depths which are away from the wind energy source (Figure 11*c*). An important aspect related to the observed inertial energy levels is the potential contribution in this energy band by the radiation of energy of inertial wave packets caused by the background vorticity fields [e.g., *Mooers*, 1975*a*, *b*; *Weller*, 1982; *Weller and Halpern*, 1983; *Briscoe and Weller*, 1984; *Kunze*, 1985]. The spectra will be considered again in the discussion section.

Photosynthetically available radiation (PAR) (Figures 8 and 9*a*) is modulated primarily by incident solar radiation (see shortwave radiation in Figure 4) at the diurnal and synoptic time scales. Cloud cover, which modulates the synoptic variability of PAR, is quite variable during period 1; however, PAR values are on average greater than those occurring during periods 2 and 3. During period 4 (JD 102), a significant increasing trend prevails because of the seasonal cycle. PAR values decay approximately exponentially with depth. The 1% light level depth (where PAR is 1% of its surface value) is shown in Figure 6. The 1% light level resides between ~80 and 100 m during the first two thirds of the period) but then deepens from ~100 to 130 m during the last 3 days of the period (extrapolated values are used below 100 m). Coincident with the deepening of the 1% light level, the mixed layer depth also increases rapidly.

Time-depth contours of beam attenuation coefficient and chlorophyll fluorescence are shown in Figures 10*e* and 10*f*. A subsurface maximum in the beam attenuation coefficient is present during the first half of this period (at ~25 m); however, beam attenuation becomes relatively uniform with depth and decreases thereafter. A subsurface maximum in chlorophyll fluorescence persists throughout the period and is located between 50 and 65 m (Figure 10*f*).

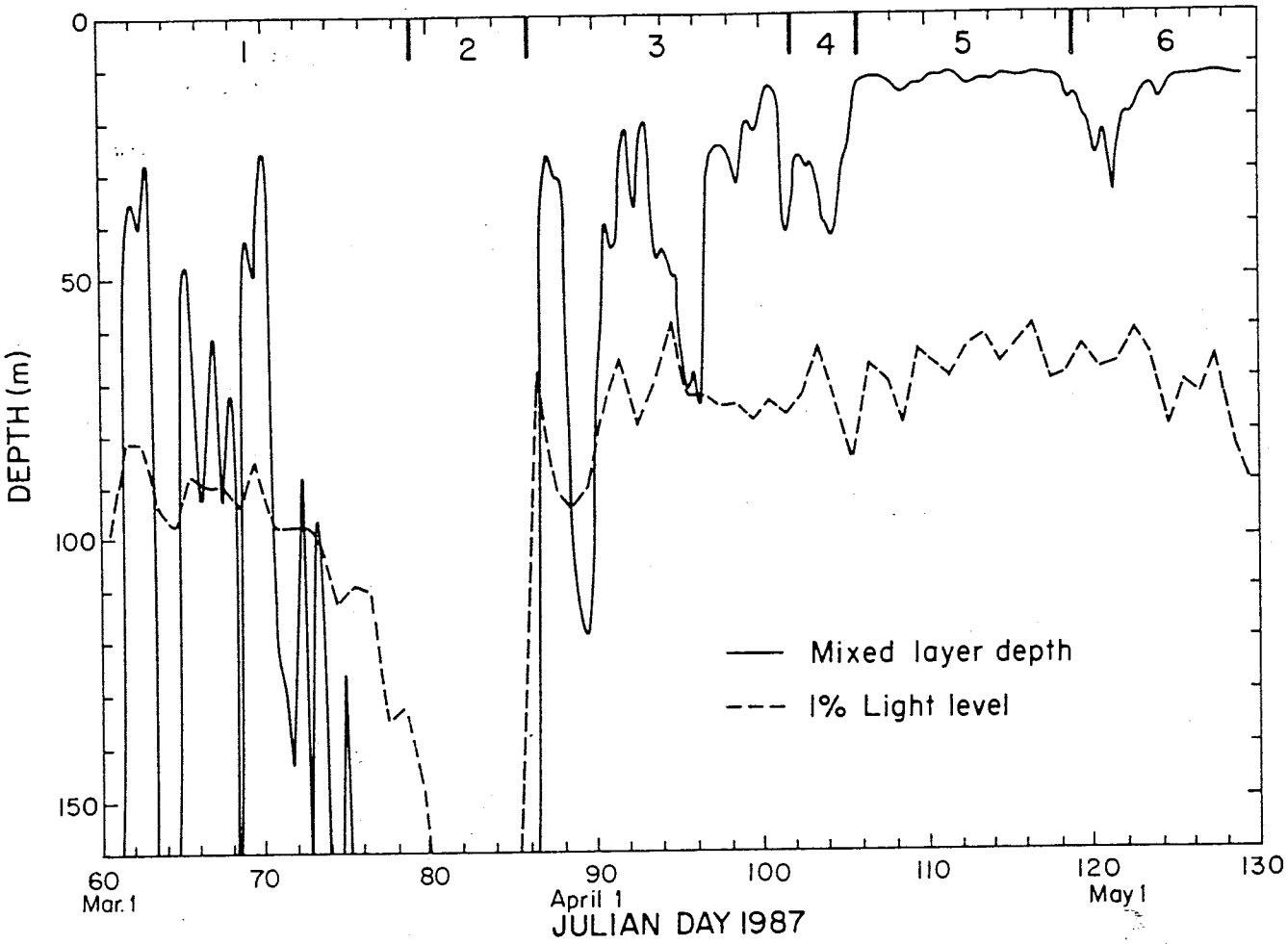

Fig. 6. Time series of the mixed layer depth and the depth of the 1% light level (PAR). The mixed layer depth is defined here as the depth at which the temperature is 0.1°C cooler than the surface temperature. At times, the mixed layer depth and the 1% light level exceeded 160 m, the greatest depth of our observations.

The time series of the bio-optical variables are shown in Figure 8 for the 23 m instrument and for all depths in Figure 9. The most obvious features are the diurnal variations in PAR, beam attenuation, and chlorophyll fluorescence in the euphotic layer. The spectra of beam attenuation and chlorophyll fluorescence show significant maxima at the diurnal period for the measurements at 23 m, but not at 101 m as indicated in Figures 11*e* and 11*f*. The diurnal signal is significant and relates to the processes of photosynthetic production, photoadaptation, and photoinhibition of phytoplankton and their loss from the upper layer through grazing by zooplankton. Effects of variations in cell refractive index and size may be important as well [e.g., *Ackleson et al.*, 1990]. It is expected that the diurnal rhythm would be minimal, if not absent, below the 1% light depth. The diurnal rhythm in beam attenuation coefficient, chlorophyll fluorescence, and dissolved oxygen time series has been examined by *Hamilton et al.* [1990], who show that the diurnal signal in beam attenuation is statistically significant through the euphotic zone (essentially from the surface to the depth of the 1% light level).

Time series of band-passed (20 - 28 hours) values of the beam attenuation coefficient, chlorophyll fluorescence, and dissolved oxygen were computed by *Hamilton et al.* [1990]. They found that both beam attenuation coefficient and dissolved oxygen generally tend to peak near sunset and reach minima toward sunrise. A combination of particle production through phytoplankton cell production during the day, and nighttime particle losses through zooplankton grazing, could lead to this cycle [e.g., *Siegel et al.*, 1989]. *Hamilton et al.* [1990] found that the diurnal signals in beam attenuation and dissolved oxygen are generally in phase for all depths within the euphotic layer, which is expected if net particle production and net dissolved oxygen production are linked through daily (sun forced) cycles of photosynthesis. Chlorophyll fluorescence generally peaks soon after sunrise at 20m and somewhat later at greater depths.

Period 2: Julian Days 79-86, March 20 to 27, 1987

The second period is distinguished by a very deep mixed layer (virtually isothermal through ~160 m) consisting primarily of 18° mode water [e.g., *Worthington*, 1959]. The euphotic zone is also quite deep (>160 m). Currents are low and advective effects appear to be negligible. Also, the water is clear (low values of beam attenuation coefficient) throughout the upper 60 m.

During this interval, the wind speeds are very low at the beginning and the end, peaking about halfway through the period at about 12 m s^{-1} ($\tau = 0.2$ Pa) on JD 82 (Figure 4). On JD 81 there are also relative minima in daily peak solar insolation and net heat flux (Figure 4). The water column temperature is nearly uniform (~18.4°C) with depth from JD 79 through JD 86 (Figures 5 and 10*a*). Stratification is quite low during this period; however, the

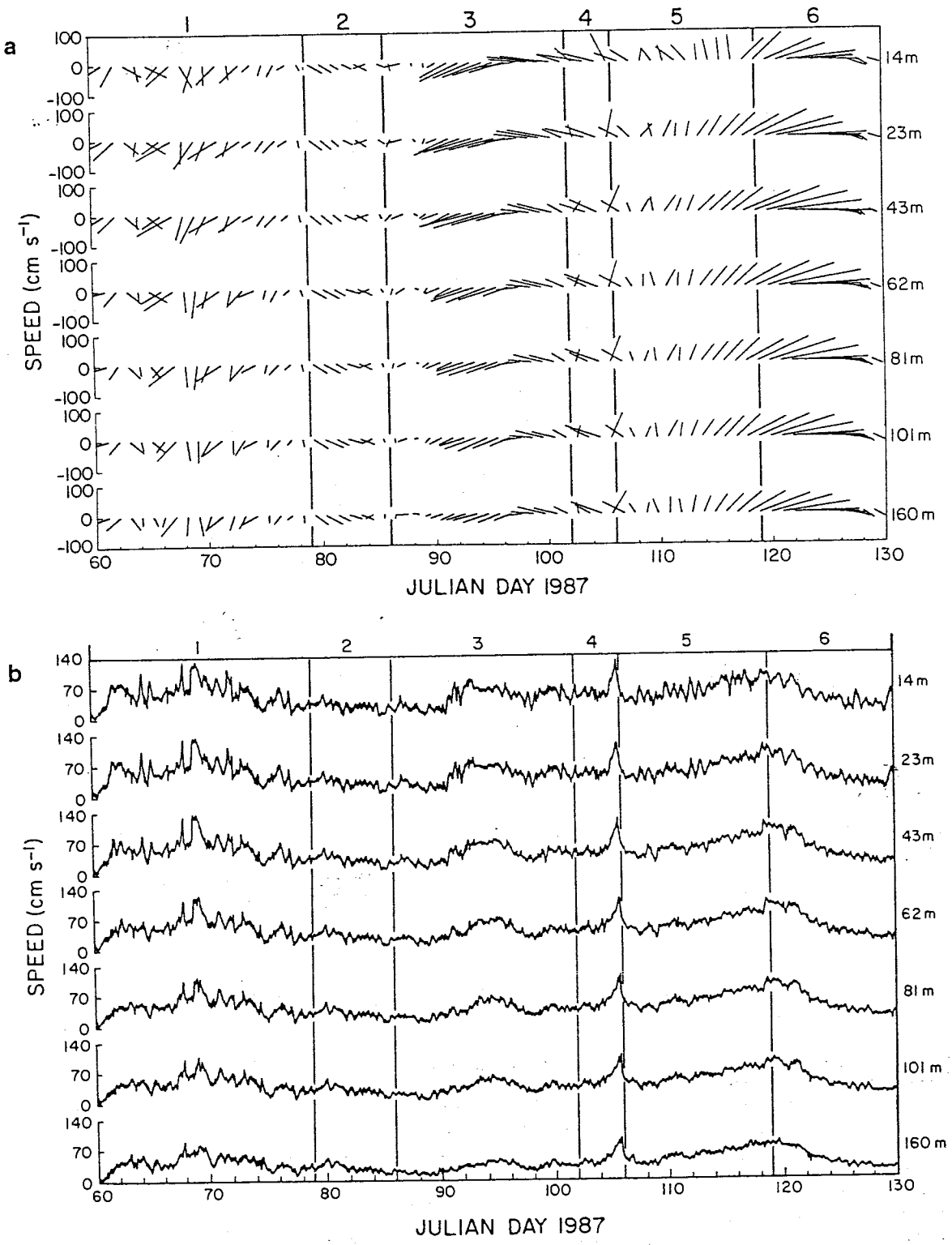

Fig. 7. Time series of (*a*) daily averaged vector currents (in cm s^{-1}), (*b*) 2-hour filtered speed at 7 depths (in cm s^{-1}), and (c) 2-hour filtered current shear (in s^{-1}).

mixed layer shoals dramatically from >160 m to ~25 m during JD 86 (Figure 6). There appears to be little variability associated with advection during this period as opposed to the first period. This is qualitatively consistent with the NOAA sea surface temperature map for JD 84 (Figure 3). The currents (Figures 7*a* and 7*b*) are generally toward the southeast with mean speeds of ~45 cm s^{-1} near the surface decreasing to about 30 cm s^{-1} at 101 m. Shear is generally lower for this period, particularly below 40 m, than for any of the other periods which is consistent with the apparent lack of significant vertical stratification or horizontal advection variations (Figures 7*a*, 7*b*, and 7*c* and Figures 10*a* and 10*d*).

PAR (Figures 8 and 9*a*) has some of its lowest values for this period. This is caused primarily by cloudy conditions. The depth of the 1% light level (Figure 6) continues to increase until JD 85

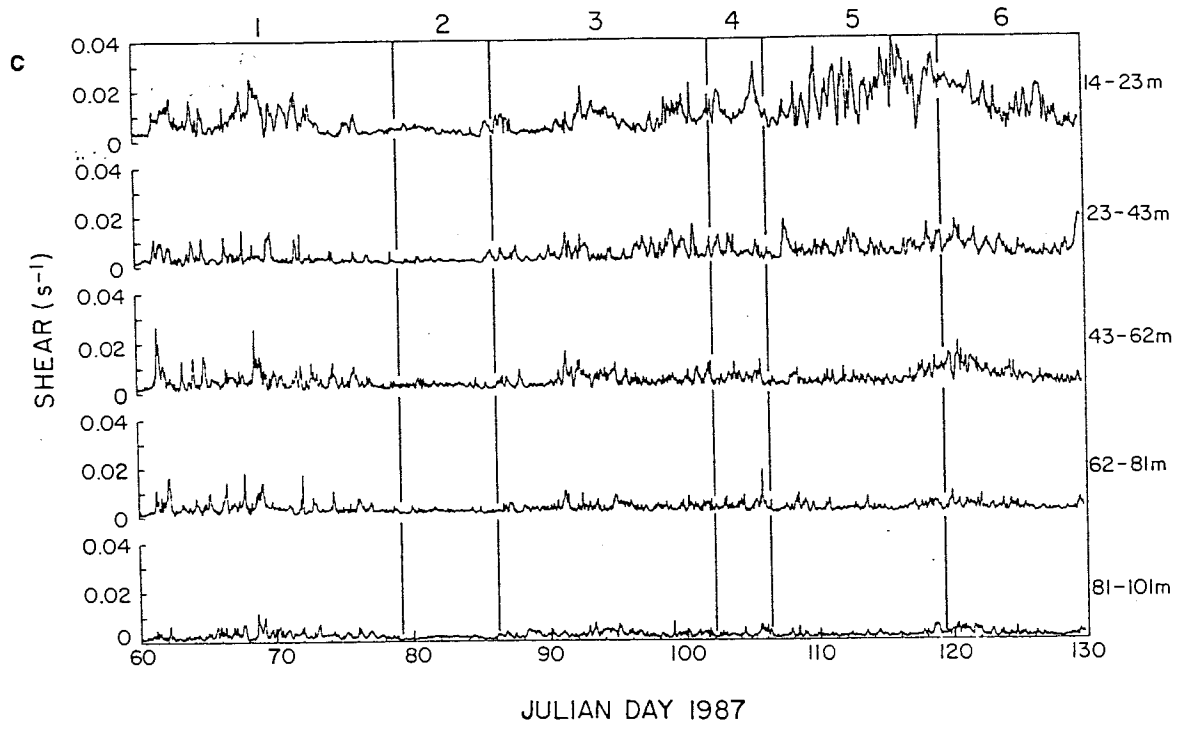

Fig. 7. (continued)

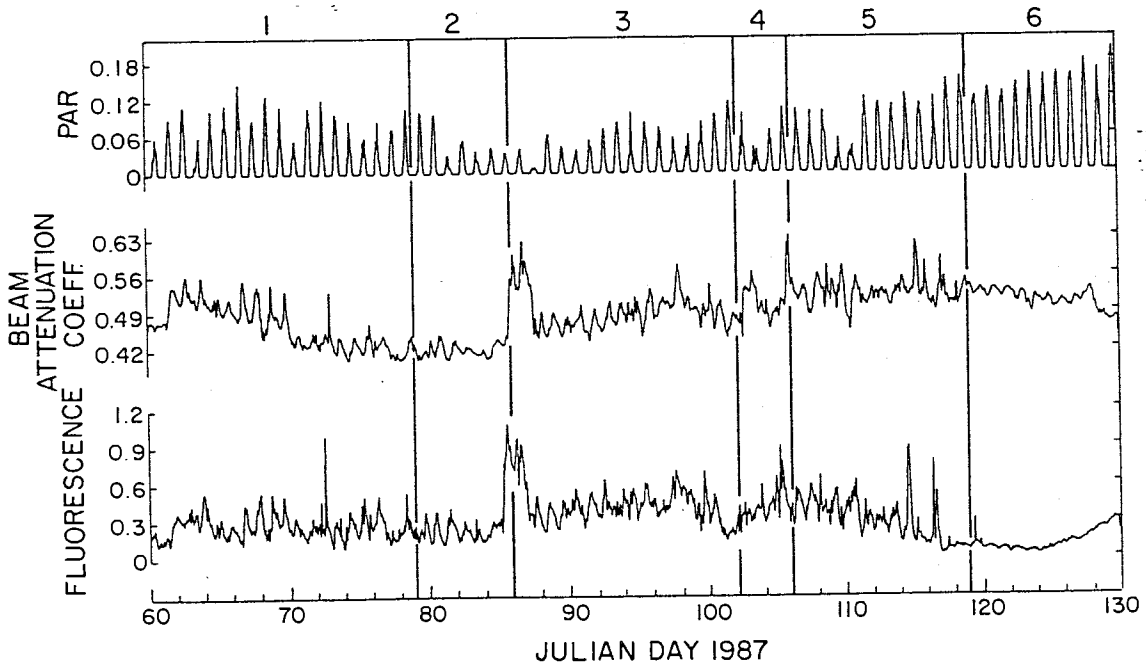

Fig. 8. Time series of PAR (in units of 10^{21} quanta m^{-2} s^{-1}), beam attenuation coefficient (in m^{-1}), and chlorophyll fluorescence (in μg Chl-*a* L^{-1}) taken from the 23 m MVMS. A 2-hour filter was used.

when it shoals rapidly from >160 m to ~70 m. This is coincident with the rapid shoaling of the mixed layer and a dramatic increase in the spectral diffuse attenuation coefficient at 488 nm wavelength (from ~0.040 to 0.075 m^{-1}; [*Smith et al.*, this issue]). Values of beam attenuation coefficient and chlorophyll fluorescence are quite low and nearly uniform with depth during most of this period. However, both begin to increase rapidly in the upper 70 m toward the end of the period (~JD 86). Subsurface maxima in beam attenuation coefficient (at ~25 m) and chlorophyll fluorescence (at ~60 m) begin to intensify as well (Figures 10*e* and 10*f*).

The most apparent feature in the bio-optical time series in the upper layer is again the diurnal cycle (Figures 8 and 9). This rhythm is most pronounced at depths shallower than 100 m (see spectra in Figures 11*e* and 11*f*). The phase relations between PAR, beam attenuation coefficient, and chlorophyll fluorescence are similar to those of period 1.

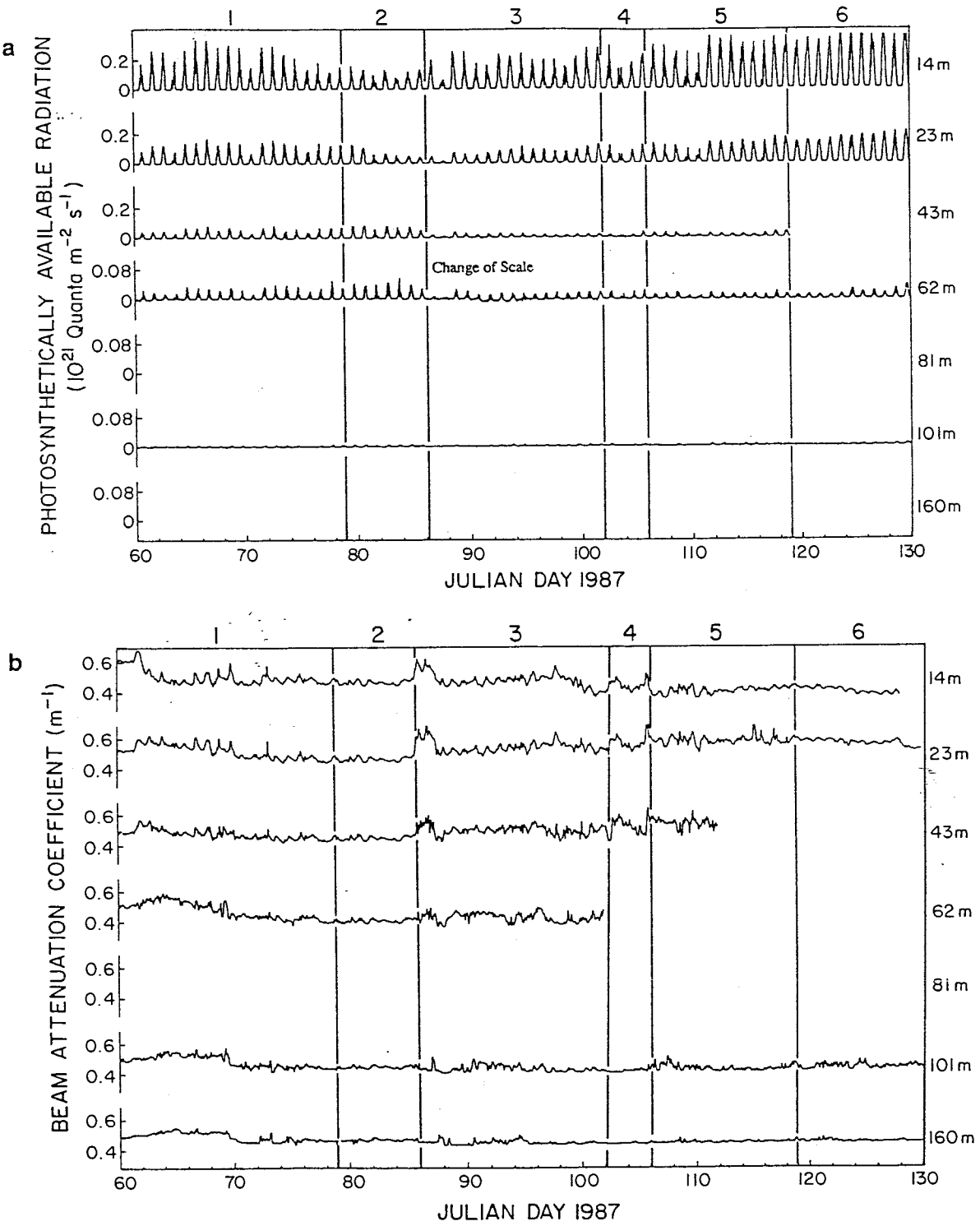

Fig. 9. Time series of bio-optical variables (2 hour filtered) at several depths: (a) photosynthetically available radiation (PAR), (b) beam attenuation coefficient, and (c) chlorophyll fluorescence.

Period 3: Julian Days 86-102, March 27 to April 12, 1987

The third period is marked by a rapid shoaling of the mixed layer and the 1% light depth. A short-lived but large phytoplankton bloom episode appears to be related to either the onset of the springtime stratification or the advection of high-biomass waters. Subsurface maxima in chlorophyll fluorescence and beam attenuation coefficient form during this period, and both quantities increase rapidly during the first few days (Figures 10*e* and 10*f*). Currents are low prior to the bloom episode and during the first third of this period, however, strong clockwise rotating currents then begin and persist throughout the remainder of the deployment.

The wind speeds are moderate and relatively persistent (averaging ~8 m s^{-1} or $\tau \sim 0.1$ Pa, Figure 4) during the period. The daily mean net heat flux is nearly constant, interrupting the heating trend

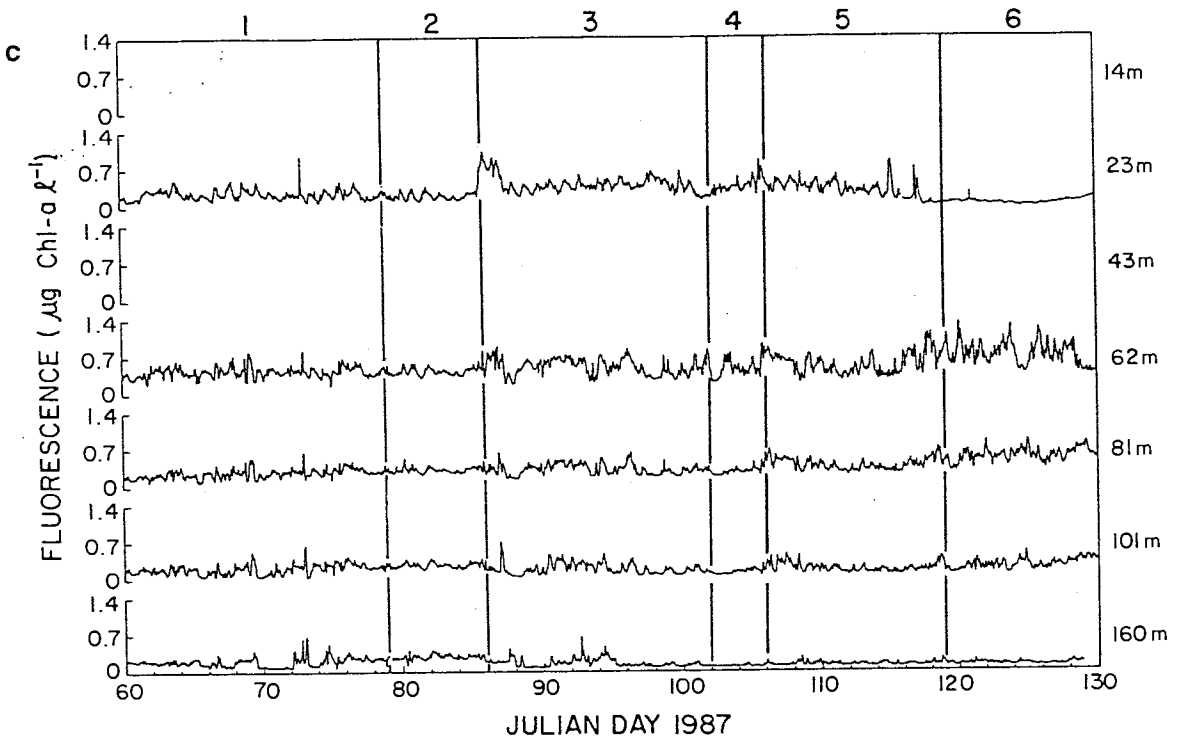

Fig. 9. (continued)

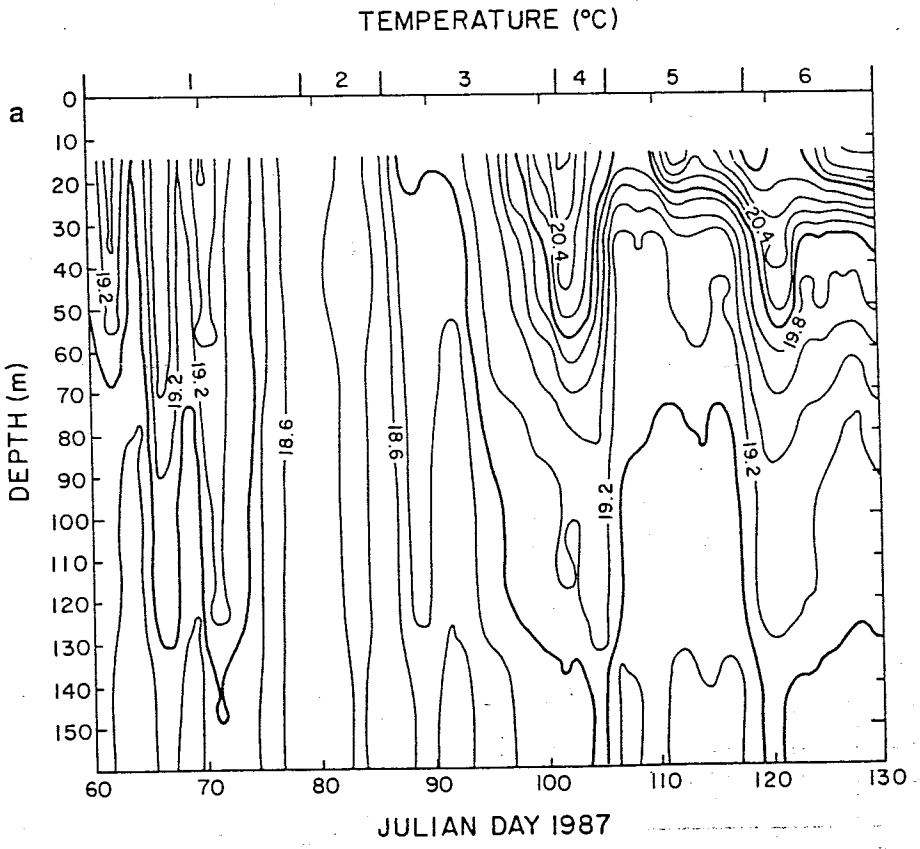

Fig. 10. Time versus depth contours: (*a*) temperature (°C), (*b*) vertical temperature gradients (°C m^{-1}), (*c*) current speed (cm s^{-1}), (*d*) current shear (s^{-1}), (*e*) beam attenuation coefficient (m^{-1}), and (*f*) chlorophyll fluorescence (μg Chl-*a* L^{-1}). A 24-hour filter was applied before contouring.

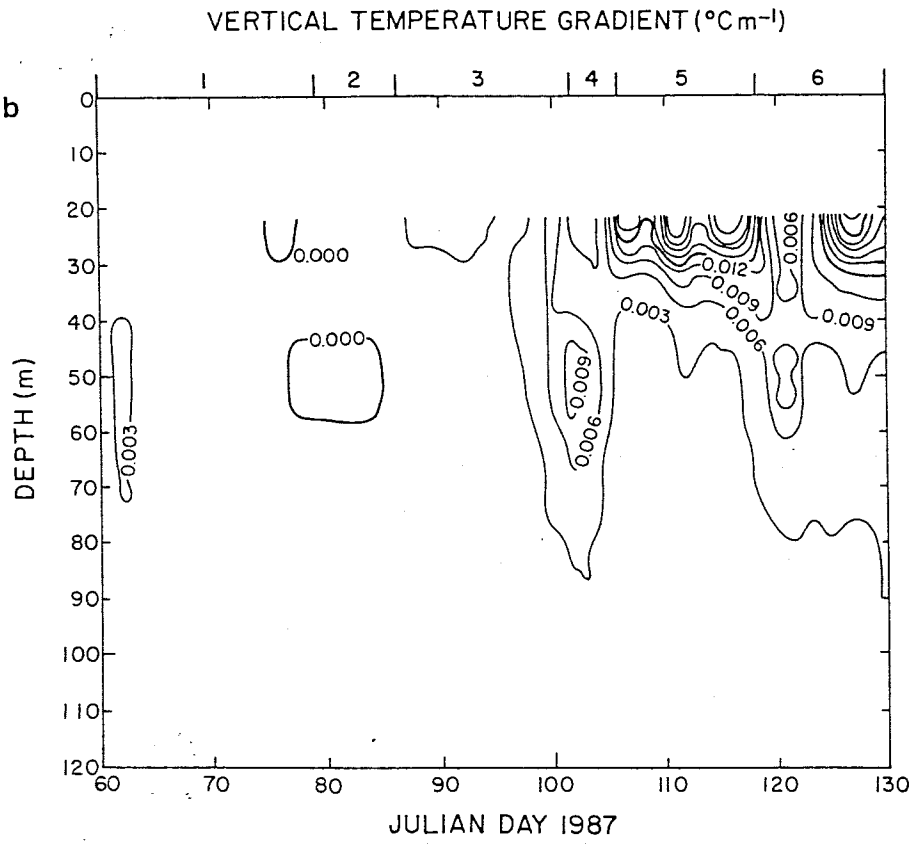

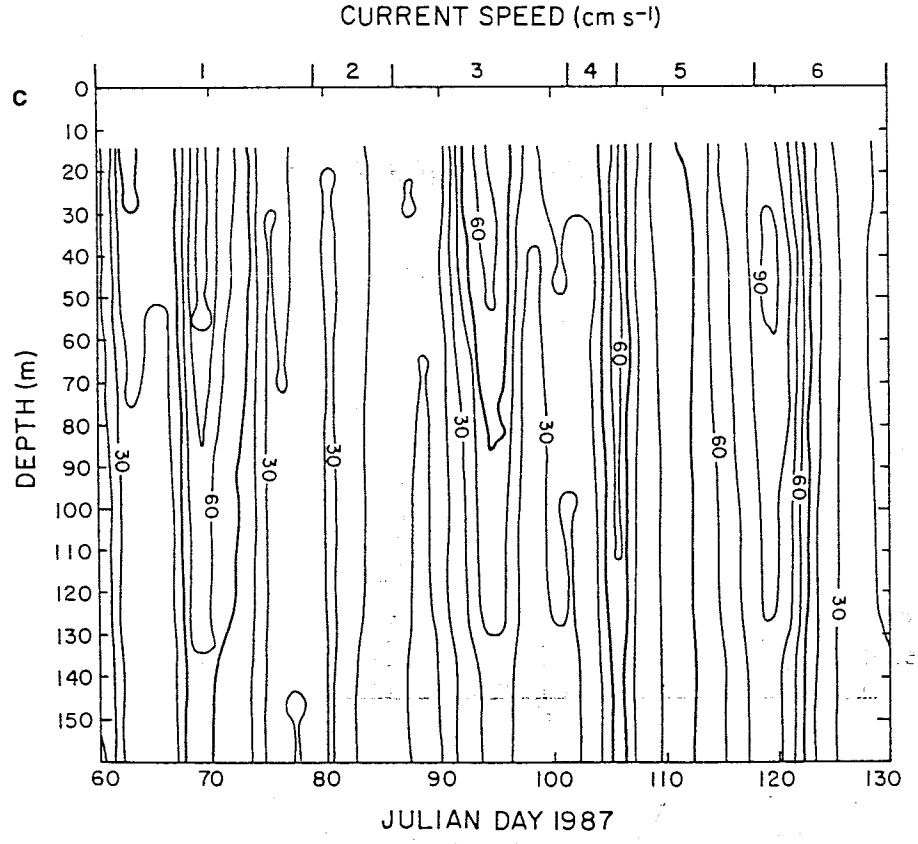

Fig. 10. (continued)

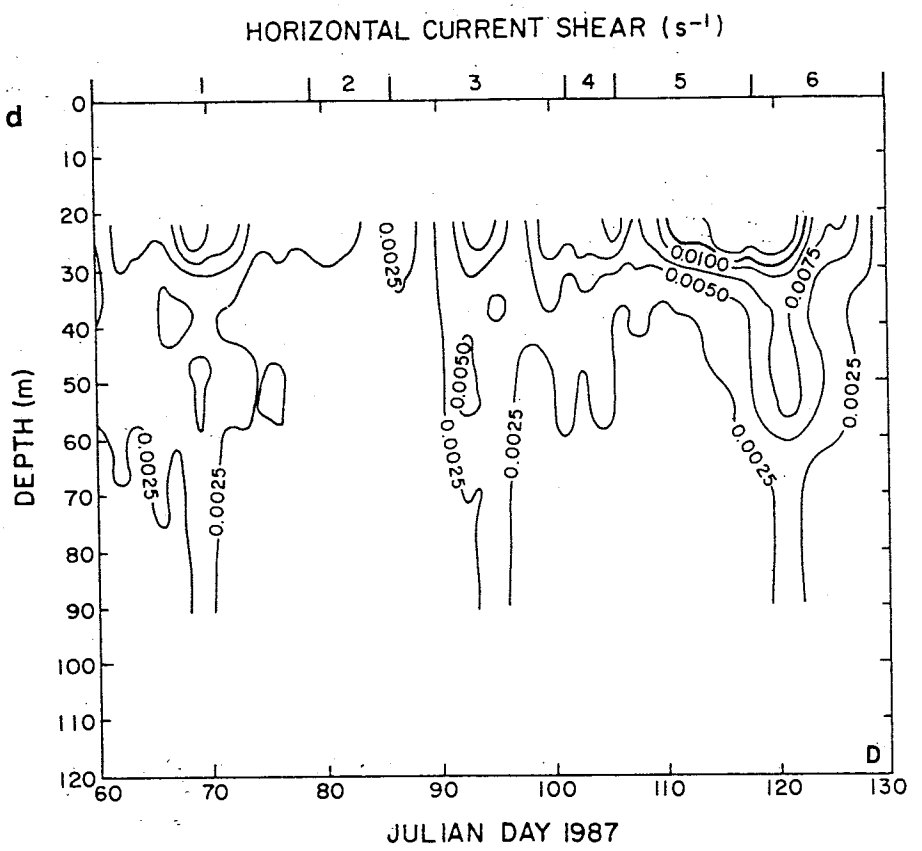

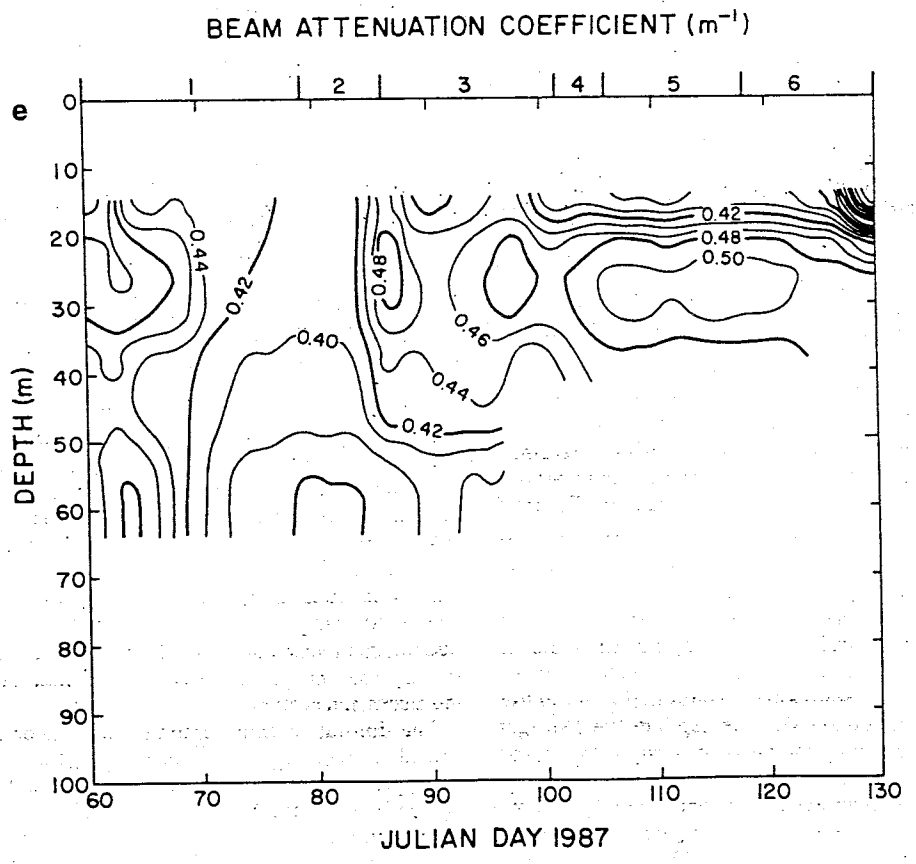

Fig. 10. (continued)

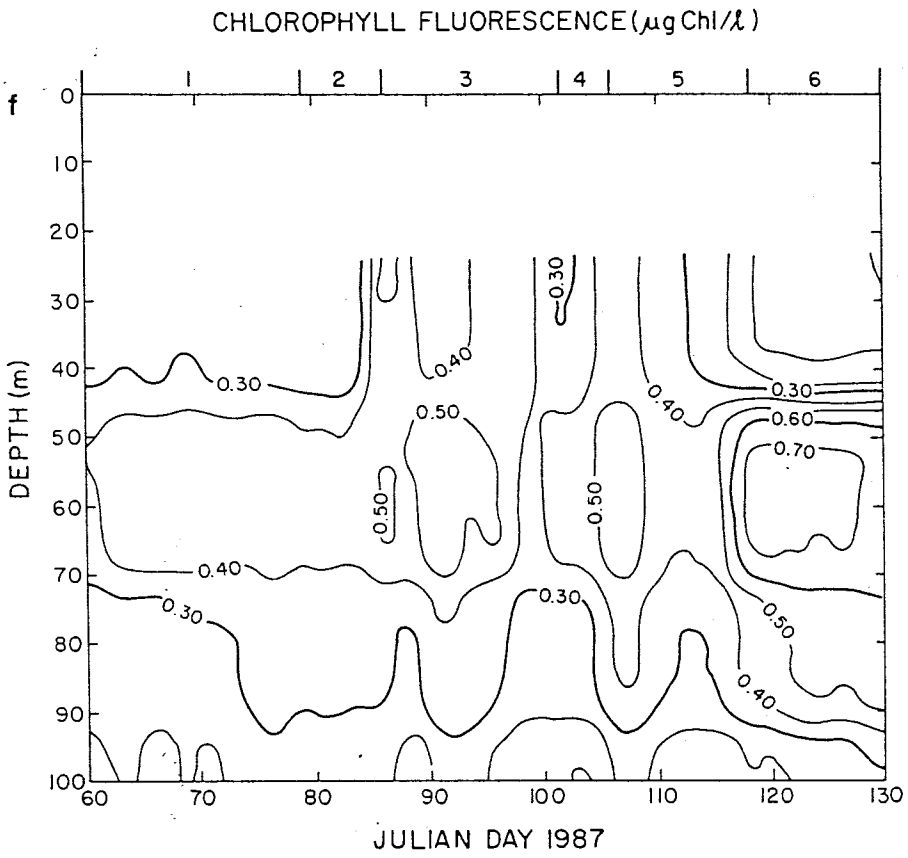

Fig. 10. (continued)

prior to and after this period. Seasonal stratification is clearly manifest at the site during this period (Figure 6). In addition to the long term trend in stratification, there are temporal variations in temperature at all depths This is similar to that described for period 1, and is presumably associated with mesoscale advection, local wind, and heat exchange fluctuations at the site. The cold core ring is moving toward the mooring as is indicated in Figure 3 (see JD 84 and 96 maps). There appears to be advection of warm outbreak water (possibly associated with the surface streamers from the cold core ring) toward the mooring site. This may account for some of the variations observed during the latter two thirds of the period.

Over the course of this period, the currents (Figures 7*a* and 7*b*), which begin toward the southwest, rotate in a clockwise direction. The maximum speed occurring during this period is about 80 cm s^{-1} at 23 m, decreasing with depth. Shear is generally increasing, particularly above 40 m, for this period and the remaining periods with a general correspondence to increasing stratification (Figures 5 and 10*d*). It is important to note that some of the lowest current values (1-5 cm s^{-1} in the upper 40 m) occur toward the end of period 2 and the beginning of period 3 (Figure 7).

The photosynthetically available radiation (Figures 8 and 9*a*) is greater during period 3 than during period 2 (by factors of 1.5 to 2.0), but less than during period 1. It should be noted that the lowest values of PAR and shortwave radiation for the entire observational period occur on JD 88. The depth of the 1% light level rises to 60-70 m following the rapid shoaling of the mixed layer and the rapid increases in both the beam attenuation coefficient and chlorophyll fluorescence. It then generally remains in this depth range. Subsurface maxima are evident in both beam attenuation coefficient (~25 m) and chlorophyll fluorescence (~60 m) as shown in Figures 10*e* and 10*f*. The daily peak values of these variable fields decline and then increase again during this period (first beam attenuation coefficient and then chlorophyll fluorescence).

A dramatic bio-optical episode is apparent in the beam attenuation and chlorophyll fluorescence time series during this period. The beam attenuation coefficient and chlorophyll fluorescence increase from values of c=0.42 to 0.60 m^{-1} and Chl-a=0.2 to 1.1 μg l^{-1} between JD 84 and 87 at a depth of 23 m (Figure 8). The increase is evident through a depth of 100 m (Figures 9*b*, 9*c*, 10*e*, and 10*f*); however, the magnitudes of the changes are greatest within the upper 40m. This bio-optical episode coincides with the onset of stratification.

The currents are very low just prior to the bloom episode, suggesting that the feature may have been local in origin. After beam attenuation and chlorophyll fluorescence peak, there is a rapid decrease in these variables followed by a general increase (most rapid for beam attenuation). The large episode appears to be reflected in all near surface bio-optical variables measured with the MVMS and in the spectral diffuse attenuation coefficient data taken simultaneously with the BOMS [*Smith et al.*, this issue]. The BOMS spectral diffuse attenuation coefficient time series were computed using spectral downwelling (vector) irradiance with instruments located at 33 and 52 m. Two alternate hypotheses for the large bloom episode (~JD 86) and its cessation are presented in the discussion section.

The diurnal rhythm continues as a major feature in the bio-optical variables (beam attenuation and chlorophyll fluorescence) in the upper layer (Figures 8 and 9). On JD 86, the diurnal variability is greatly enhanced for 2 days coinciding with the rapid onset of stratification. Again, this rhythm is most pronounced at depths shallower than 100 m. The phase relationships between beam attenuation, dissolved oxygen, and chlorophyll fluorescence generally remain unaltered from those observed during period 2.

Period 4: Julian Days 102-106, April 12 to 16, 1987

The springtime stratification persists during period 4; however, the variations are complex because both warm outbreak waters and cooler Sargasso Sea waters are observed during this period (Figure 3; JD 103). The last portion of the period is marked by considerable cooling at all depths. The site is subjected to a wind event which may cause mixed layer deepening and cooling of near surface waters, although advection of cool waters may be important as well. PAR is low for the period, and the magnitudes of the subsurface maxima in beam attenuation coefficient and chlorophyll fluorescence are less than during the preceding period.

The wind speed peaks midway through the period (peak value of ~12 m s^{-1} ($\tau \sim 0.2$ Pa), Figure 4). The net heat flux is greater during the initial and final portions of the period, as shortwave radiation is quite low in between. The seasonal evolution of stratification is interrupted, possibly by a wind event combined with a high loss of heat or by a major mesoscale feature or by a combination of the two (see Figure 4). The mixed layer depth increases prior to this period but then eventually shoals to ~12 m where it remains for the duration of period 5.

Oscillations in temperature (Figure 5) are observed during this period. A cold core ring in the vicinity of the mooring (see JD 103 in Figure 3) and the entrained warm outbreak waters associated with it are presumably responsible for the observed variability.

During this period, the currents (Figure 7) continue to rotate clockwise. The maximum instantaneous speed occurring during the entire observational period at 14 m is ~125 cm s^{-1} on JD 106. The mean 24 hour filtered currents are ~60 cm s^{-1} and relatively uniform with depth (Figures 10*c* and 10*d*). Shear is greater at depths shallower than 40 m with peak values comparable to those observed during period 1 (Figure 7). PAR values (Figures 8 and 9*a*) for the period are strongly modulated by the incident solar radiation which is low during the middle portion of the period. The 1% light level remains near 65 m. There are relatively large variations in beam attenuation and fluorescence toward the end of period 3 and during period 4. These are presumably related to the mesoscale water mass variations associated with the edge effects of the cold core ring. Variations in the beam attenuation coefficient (Figures 8 and 9*b*) and the spectral diffuse attenuation coefficient (at 488 nm [*Smith et al.*, this issue]) are highly coherent at ~40 m. Subsurface maxima in beam attenuation coefficient and chlorophyll fluorescence intensify at depths of ~30 and 60 m, respectively (Figures 10*e* and 10*f*).

The diurnal rhythm in the bio-optical variables (PAR, beam attenuation, and fluorescence) is less apparent during this period

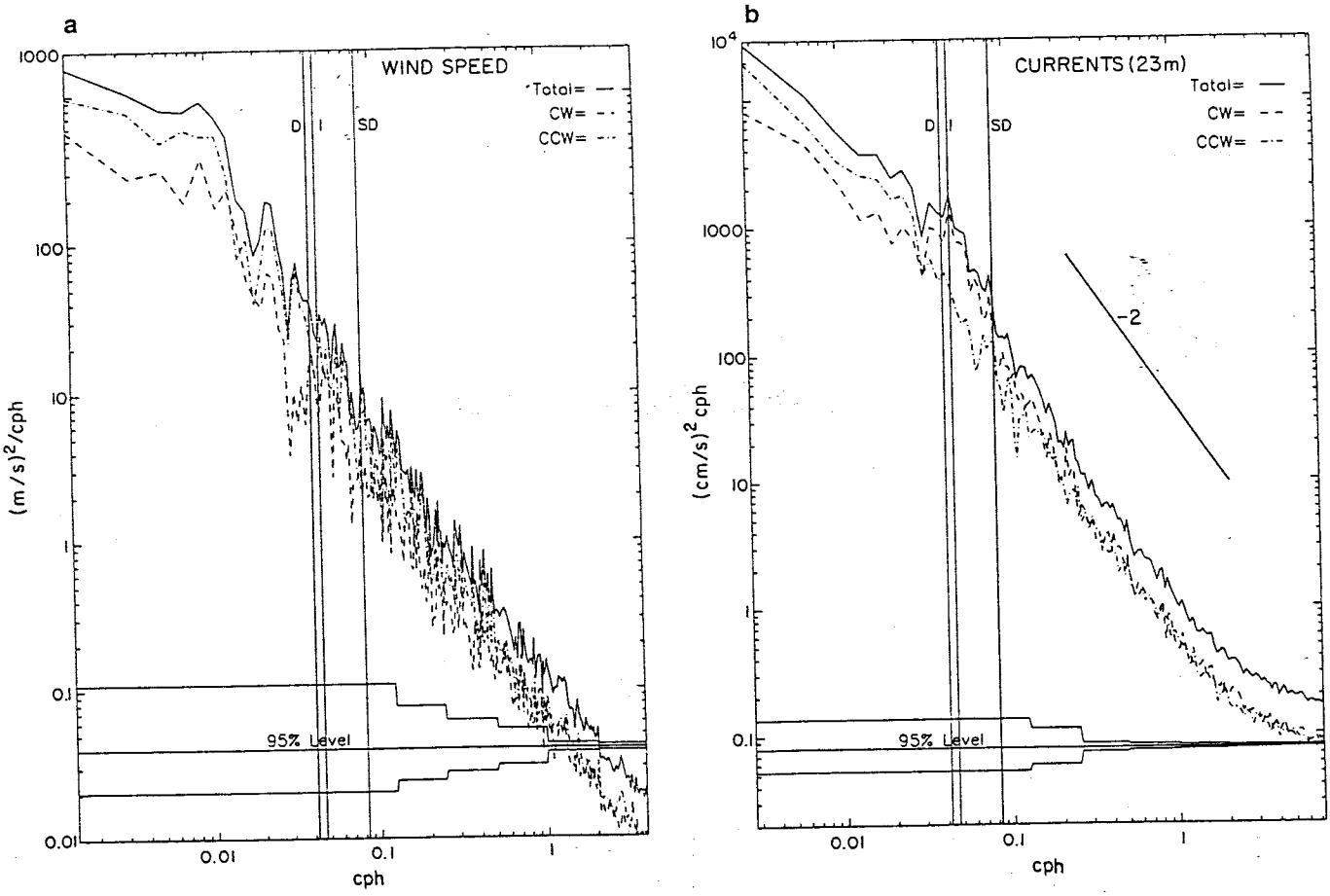

Fig. 11. Rotary spectra of horizontal components of (*a*) wind speed, (*b*) currents at 23 m, and (*c*) currents at 101 m, and spectra of (*d*) temperature, (*e*) beam attenuation coefficient, and (*f*) chlorophyll-*a* fluorescence at 23 and 101 m. CW and CCW indicate clockwise and counterclockwise components of the rotary spectra, and D, SD, and I indicate diurnal, semidiurnal, and inertial frequencies, respectively. The local inertial period is 21.5 hours. The 95% confidence limits are also represented. The -2 slope represents the power law for internal gravity wave spectra [*Garrett and Munk*, 1972].

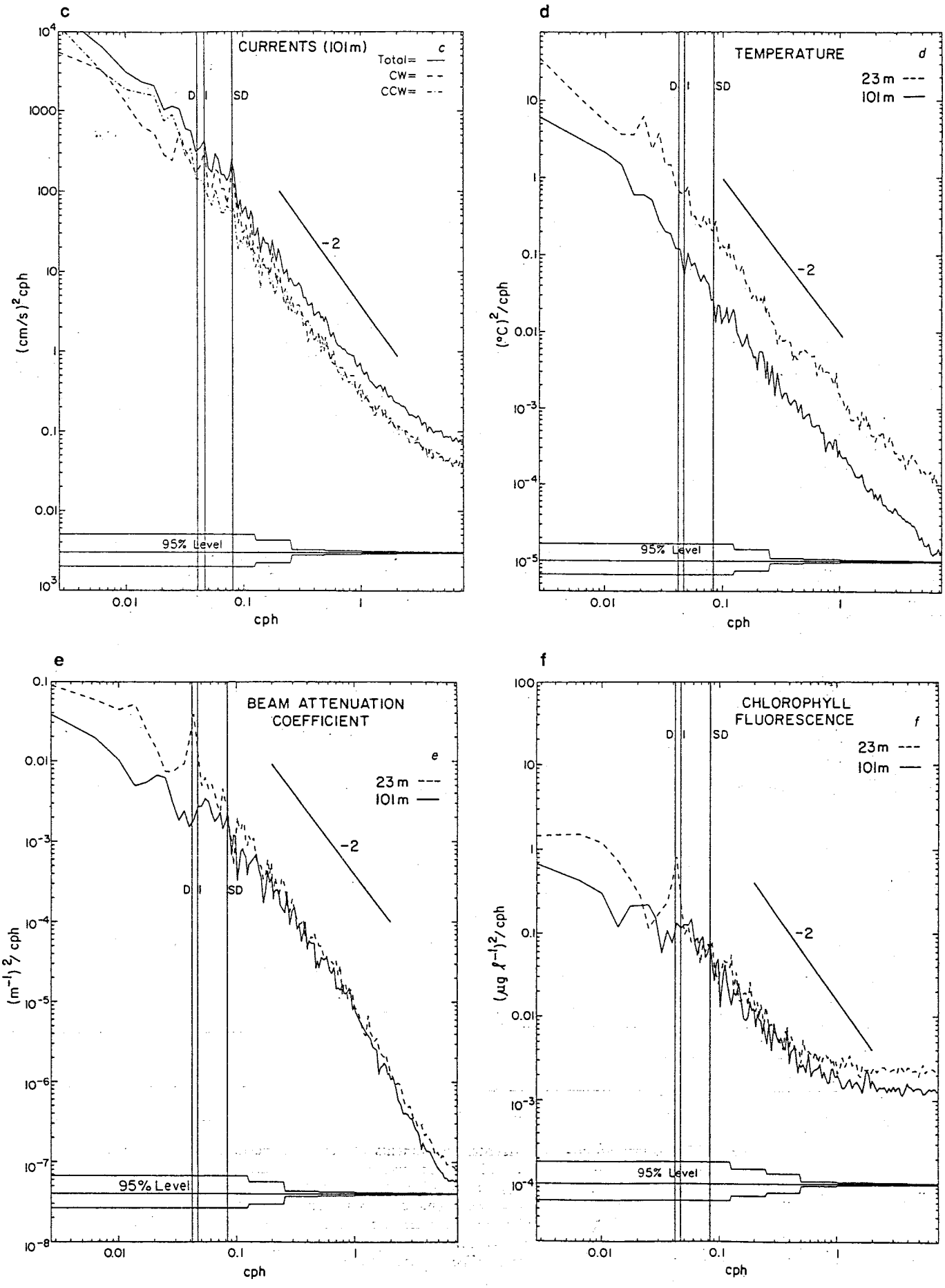

Fig. 11. (continued)

than the others, presumably because of the great mesoscale variations (Figures 8, 9, and 10). However, diurnal phase and amplitudes are essentially unchanged from the previous period.

Period 5: Julian Days 106-119, April 16 to 29, 1987

Following the cooling during period 4, a warming trend at all depths prevails during period 5. Resumed stratification is apparent above 40 m. The mooring site is near the boundary between warm outbreak waters and cooler Sargasso Sea waters (Figure 3) which would explain the observed large excursions in near-surface temperature. PAR values generally increase, particularly after the first half of the period. The near-surface waters continue to be somewhat clearer and lower in pigment biomass; however, the subsurface maxima in beam attenuation coefficient and chlorophyll fluorescence intensify somewhat.

The wind speeds are generally lower (averaging ~8 m s^{-1} or τ ~ 0.1 Pa; Figure 4) and the net heat flux is generally greater during this period compared with the previous ones. The combination of these two effects contributes to the resumed local heating of the upper layers, with the heating rate being comparable to that of period 3. Consequently, the seasonal stratification intensifies again (Figure 10*b*). The mixed layer depth is relatively constant at a depth of ~12 m. Again, some mesoscale structure is evident in the temperature time series (Figures 5 and 10*a*).

The cold core ring continues to move southward, and warm outbreak waters associated with the circulation of the cold core ring appear to advect through the mooring site (see JD 114 of Figure 3 and JD 112 of Figures 5 and 10*a*). The variations in the temperature records are presumably associated with this feature. Stratification is particularly intense in the upper layer during this interval. During this period the currents (Figure 7) are qualitatively consistent with the advection implied by the NOAA sea surface temperature maps (see JD 114 map). There is veering of the currents to the right (~30 - 45°) with depth within the upper 40 m. However, the currents are generally aligned at greater depths. The current speeds gradually increase during the period to values of ~100 cm s^{-1} in the upper 100 m on JD 119. Shear between 14 and 23 m reaches its greatest values with the increase following the general current speed trend. The current structure is most likely dominated by the cold core ring.

PAR (Figures 8 and 9*a*) is consistent with the incident shortwave radiation and gradually increases during the period reaching values exceeding the greatest values up to that point in the time series. The 1% light level remains near 65 m during this period. The subsurface maximum in beam attenuation coefficient (at ~30 m; Figure 10*e*) continues. The chlorophyll fluorescence maximum begins to intensify rapidly toward the end of this period, particularly at a depth of 62 m (Figure 9*c*).

During this period, chlorophyll fluorescence generally declines at 23 m. The diffuse attenuation coefficient at 488 nm determined from BOMS at 33 and 52 m increases slightly [*Smith et al.*, this issue]. One possible explanation for this could be that the sustained high levels of PAR led to photoinhibition of the fluorescence response by phytoplankton at high light excitation, leading to the observed reductions in chlorophyll fluorescence. This effect is consistent with the observed maximum in beam attenuation coefficient and the minimum in chlorophyll fluorescence at ~20 m occurring on JD 106. At depths greater than ~40 m, there are no appreciable long term changes in the beam attenuation coefficient or chlorophyll fluorescence. Beam attenuation coefficient and dissolved oxygen concentration continue to peak near sunset at all depths.

Period 6: Julian Days 119-130, April 29 to May 10, 1987

The mooring site is near the edge of warm outbreak waters, but it appears to be primarily within Sargasso Sea waters during this period (Figure 3). Near-surface stratification and temperatures increase following a brief deepening of the mixed layer, apparently in response to a wind event. The currents are strong in the beginning of the period but decrease with time and continue their clockwise rotation. PAR increases during the period to the highest levels of the deployment, while near-surface beam attenuation coefficient and chlorophyll fluorescence decrease. However, the subsurface maxima of these variables intensify during the early portion of the period.

The wind speeds are relatively low (averaging ~8 m s^{-1} or τ ~ 0.1 Pa; Figure 4) except for a modest wind event on JD 120. The net heat flux is generally greater during this period and the preceding period than the earlier periods. Again, these two effects contribute to the continued general heating of the upper layer. A wind event and low surface heat input occurring on JD 120 retard the heating of the surface layer. The mixed layer, which is ~15 m in depth, responds by deepening to ~30 m.

During this period, the cold core ring moves south-southwestward between JD 114 and JD 121, placing the mooring near the western edge of the cold core ring and the edge of warm outbreak waters (see JD 121 of Figure 3). The currents (Figure 7) continue to rotate clockwise. The currents progress in direction, beginning toward the northeast and ending toward the east-southeast. Qualitatively, the current direction implied by the NOAA sea surface maps (see JD 114 map) is consistent with the current meter data. There is slight veering of the currents to the right (a few degrees) with depth between 14 and 23 m; however, the currents are roughly aligned at greater depths. Current speed and current shear decrease at all depths after JD 119 (Figures 10*c* and 10*d*), following a peak in currents of ~80 cm s^{-1}. Once again, the current structure is regulated by the cold core ring which stays in close proximity to the mooring and the warm outbreak waters associated with the ring.

PAR (Figures 8 and 9*a*) continues to increase during the period and reaches the greatest values observed during the deployment. The depth of the 1% light level deepens by ~20 m between the end of period 5 and the end of period 6. This is consistent with the decreasing near surface values of beam attenuation coefficient and chlorophyll fluorescence (Figures 10*e* and 10*f*).

Considering the 23 m time series, there is a significant reduction in the high-frequency variability of beam attenuation coefficient and chlorophyll fluorescence during this period. Values of beam attenuation and chlorophyll fluorescence at 23 m are comparable to values obtained at the very beginning of the deployment almost 2 months earlier, which may suggest that biofouling of the optical instruments was not significant. The subsurface maxima of the beam attenuation coefficient and chlorophyll fluorescence intensify during the early portion of the period before declining midway through the period. Thus it appears that significant changes in the vertical structure of the pigment (chlorophyll fluorescence) and particle concentrations have occurred. This aspect is important in terms of interpreting satellite determinations of pigment biomass as discussed below. Again the diurnal rhythm in the bio-optical variables is present and the phase relations remain as they were in the preceding period. However diurnal amplitudes in beam attenuation coefficient and chlorophyll fluorescence at 20m are greatly reduced compared to all previous periods. This aspect and other details concerning diurnal variability are discussed by *Hamilton et al.* [1990].

4. DISCUSSION

The cycle of seasonal insolation and its accompanying wind forcing dominate the physical structure of the upper layers of the Sargasso Sea as indicated in the evolution of the mixed layer and the seasonal thermocline. In addition, mesoscale advective features are important for both the physics and the bio-optics. Two alternate hypotheses are forwarded for the observation of the large bloom episode occurring between JD 86 and 89. The first is the

Sverdrup spring bloom hypothesis and the second concerns advection of high biomass. These two alternate hypotheses are discussed below.

The extremely short time scale for the seasonal shoaling of the mixed layer and the 1% light level is striking. It appears that these phenomena may be related through a short-lived bloom episode (beginning on JD 86) which may have been locally produced. The coincidence of the seasonal stratification with the increase in beam attenuation and fluorescence along with the diffuse attenuation coefficient data suggests a spring bloom phenomenon. The classical explanation of this effect [e.g., *Sverdrup*, 1953] is that the winter period is characterized by deep mixing. In this case, respiration exceeds photosynthesis in phytoplankton because vertical excursions take them out of the euphotic zone. With stratification in the spring, the vertical excursions of phytoplankton are restricted and they are exposed to higher light levels, production exceeds respiration and grazing loss, and phytoplankton reproduce in large numbers. Hence a bloom can occur within a short period of time once the proper environmental conditions are presented. It is possible that the dramatic episode occurring between JD 86 and JD 89 can be explained at least in part by this process. The Sverdrup spring bloom hypothesis assumes a nonadvective situation, meaning that the bloom phenomenon occurs as a result of local conditions. The currents prior to the episode are toward the southeast, and some of the lowest current speeds (1 - 5 cm s^{-1}) occur during the episode. The bloom episode appears to have been manifest at all depths in the water nearly simultaneously, perhaps with some lag with depth, and its effects decrease with depth. Although the daily mean light levels were relatively low prior to the bloom, the 1% PAR depths were greater than 160 m. Thus with ample nutrients and light exposure following incipient stratification, conditions may have been optimal for rapid phytoplankton growth rates.

Following the large bloom episode, the beam attenuation and fluorescence decrease rapidly, but then they gradually increase later during period 3. The decline could result from a transition to a nutrient- or light-limited situation. No nutrient time series data were taken; however, PAR reached its lowest daytime values for the entire deployment about 2 days after the onset of the bloom and nearly coincident with the rapid decline of chlorophyll fluorescence and beam attenuation. The later recovery in chlorophyll fluorescence and beam attenuation could be explained by the return of high light levels and the transport of additional nutrients into the euphotic zone through episodic wind mixing along with the continuation of the relatively shallow mixed layer. It is not known what role zooplankton grazing plays, as no relevant zooplankton data were collected.

An alternate explanation is that waters of some undefined horizontal scale and characterized by high stratification and biomass may have advected past the mooring site. The currents are quite uniform with depth, so advection of high biomass waters past the mooring site would result in nearly simultaneous changes in chlorophyll fluorescence and beam attenuation at depths within the euphotic zone. This effect could be manifest in an increase in biomass followed by a decrease. It is evident from the time series of temperature for the entire observational period, except for period 2, that advective processes are occasionally important on time scales of several days. However, neither the NOAA sea surface temperature maps nor the specific AVHRR imagery indicate that the mooring is influenced by a mesoscale feature prior to or during this bloom episode. Again, the current meter data indicate very low currents. If a high-biomass patch of water were advected past the mooring, it would have necessarily been quite small in horizontal scale. For example, taking the episode duration to be 2 days and the mean advection to be 1 - 5 cm s^{-1}, then the horizontal scale would have been ~2 - 9 km. The process of ventilation of 18° waters may occur with considerable horizontal heterogeneity, and historical satellite imagery of ocean color suggests that the surface manifestation of the spring bloom is generally quite patchy. The advection of such small-scale patchy waters past the mooring could possibly explain the early bloom episodes.

In-depth analyses and modeling are needed for us to understand what critical physical and biological conditions led to the episodes. However, one important aspect is the intermittent nature and very short time scale of the bloom process (<2 days) which would be virtually impossible to observe with conventional sampling instruments and strategies. Further, the need for current measurements is clear. Finally, it is possible that diurnal phase changes in bio-optical variables may be useful for determining the timing of phytoplankton successions and for monitoring local photosynthetic activity [*Hamilton et al.*, 1990].

Overall, the first deployment data show considerably more physical and bio-optical variability than those of the two later deployments because of the dynamic springtime shoaling of the mixed layer and the accompanying phytoplankton bloom and more mesoscale variability associated with Gulf Stream cold core rings and warm outbreak waters. The spectral characteristics of internal gravity waves, generally with frequencies bound by the local buoyancy frequency and the inertial frequency, have been the subject of numerous observations and models. Virtually all of this work has been limited to physical data, particularly currents and temperature. The present data set allows us to consider variability in bio-optical properties associated with internal gravity waves as well.

The rotary spectra for currents show energy near the local inertial frequency to be dominated by a clockwise rotation as expected for inertial motion in the northern hemisphere. There are some characteristics of these rotary spectra (Figures 11*b* and 11*c*) which should be noted. The average energy contained in the inertial frequency band is lower than that found in the rotary current spectra of *Briscoe and Weller* [1984], who used vector measuring current meters during the LOTUS experiment (same location as our mooring site). However, their result was obtained using an 11-month time series. Rotary spectra for the second and third deployments (not shown here) of the Biowatt experiment (corresponding to JD 135 - 325) give results for the inertial peak which are of the same order of magnitude as those obtained by *Briscoe and Weller* [1984]. In addition to a reduced inertial response, the first-deployment current spectra indicate the presence of more energy in the low-frequency mesoscale bands than is observed in the two later deployments. These same characteristics for the spring - early summer time frame were reported for the current power spectra determined with current profilers by *Eriksen* [1988], who conducted two 3.5-month time series (spring - summer and fall - winter) as part of LOTUS. The seasonal variability in the physical parameters and their interaction with the local ecological system are being studied presently.

Changes in the beam attenuation coefficient are caused primarily by variations in particle concentrations, whereas changes in chlorophyll fluorescence are caused primarily by variations in chlorophyll pigment concentrations and phytoplankton light physiology or quantum efficiency [*Kiefer et al.*, 1989]. The temporal variability of these quantities in the internal gravity wave frequency domain, as measured from a mooring, is expected to be dependent on the vertical displacement of their vertical distributions. A spectral power law can be determined from the slope of the log of the variance/unit frequency of the parameter of interest with respect to the log of the frequency. The power law relation developed by *Garrett and Munk* [1972] for currents and temperature indicates that the spectral energy density is inversely proportional to the square of the frequency in a frequency domain somewhat greater than the inertial frequency (here ~0.05 cph) and less than the buoyancy frequency (here 2 - 7 cph). The power law formalism is useful in that it characterizes the rate of transfer of internal wave energy between scales, generally from large scales (low frequencies) to smaller scales (high frequencies). Our spectra for currents, temperature, and beam transmission are in good agreement with this -2 power law. However, a power of ~-1.6 is obtained for chlorophyll fluorescence and dissolved oxygen (not

shown here). It may be argued that beam attenuation is generally acting as a passive scalar tracer, as is temperature, for the time scales relevant to internal gravity waves. Chlorophyll fluorescence measurements are subject to complications associated with time scale variability related to processes such as photoadaptation and photoinhibition and their response to light field changes due to the internal gravity wave field. The spectra of the several variable fields will be considered in more detail in a separate paper.

The time series observations of *Smith et al.* [this issue] focused on bio-optical variability in pigment biomass by measuring spectral downwelling irradiance and upwelling radiance at depths of 33 and 52 m, or between our MVMS units placed at 23, 43, and 62 m. Our measurements of pigment biomass with the MVMS were done virtually continuously (day and night) with a strobe in situ fluorometer [*Bartz et al.*, 1988]. The radiance and irradiance sensors of *Smith et al.* [this issue] require natural light, thus limiting their time series to daylight hours. They utilized three different methods to determine pigment biomass: (1) an empirical model or algorithm (here-in-after referred to as the power law model) which regresses in-water pigment concentrations against upwelled radiance ratios or downwelled irradiance ratios in different wave bands (e.g., best known for satellite estimations of pigment biomass [e.g., *Gordon and Morel*, 1983]), (2) a semianalytic model which utilizes physical and mechanistic biological relationships [e.g., *Gordon et al.*, 1988], and 3) an analytic model based on the amount of in situ fluorescence stimulated by the in situ radiance or natural fluorescence (683 nm) and PAR [*Kiefer et al.*, 1989] (here-in-after referred to as the natural fluorescence method).

For the power law model, *Smith et al.* [this issue] utilized their contemporaneous mooring and chlorophyll-like pigment (chlorophyll-*a* + phaeopigment-*a*) profile data to evaluate the relevant coefficients for their model and utilized the BOMS radiance and irradiance data to compute time series of chlorophyll-like pigment concentrations. They estimate standard errors between shipboard and BOMS power law determinations to be ±30%. It should be noted that this method gives estimates averaged over the attenuation lengths (depths) of the order of tens of meters opposed to local fixed depth estimates. The natural fluorescence method also requires natural light and is limited to daylight observations. The fluorescence quantum yield and mean chlorophyll-*a* specific absorption coefficient for the phytoplankton crop were estimated using shipboard data for the appropriate depths and applied to the mooring data. Application of the natural fluorescence method results in time series of fluorescence associated with chlorophyll-*a*-like pigment concentrations at the specific depths of the instruments.

The MVMS and BOMS determinations of chlorophyll-*a* or chlorophyll-*a*-like pigments are different on a quantitative basis for several of the reasons cited above. However, intercomparisons between the MVMS chlorophyll fluorescence time series at 23 and 43 m and the BOMS time series of chlorophyll fluorescence (based on the natural fluorescence model) at 33 and 52 m (see *Smith et al.* [this issue]; Figures 11*c* and 11*f* and our Figures 9*c* and 10*f*) show qualitative agreement. The large bloom episodes are apparent in both time series as are the general trends; however, there are differences in magnitudes. The agreement between these fundamentally different, though complementary, concurrent measurements is encouraging. It will be desirable to utilize several different methodologies in the future to address many of the important questions concerning pigment biomass, primary productivity, and carbon fluxes in the upper ocean.

It is apparent that the physical and bio-optical processes are often highly coupled, but not necessarily linearly or simply. Part of the complexity in the interpretation of our data originates with the partitioning of local versus advective effects. Determinations of time scales of relevant processes and their phases are crucial. It is absolutely critical to obtain physical data concurrently with the bio-optical data in order to interpret (e.g., partition local versus advective changes, establish physical time scales, etc.) and model the pertinent processes. In addition, many of the observations described here (e.g., PAR, chlorophyll fluorescence, beam attenuation coefficient, and dissolved oxygen) can be used as model input to generate time series of biomass, primary productivity, and carbon fluxes [e.g., Dickey, 1991].

The results presented here and by *Smith et al.* [this issue] provide new and unique information concerning the springtime evolution of bio-optical and physical properties of the upper ocean in the Sargasso Sea. The high temporal resolution observations obtained using the MVMS and the BOMS will enable much higher levels of analysis and model testing than were possible for our predecessors. Our results indicate that undersampling (and aliasing) should be of considerable concern to researchers who desire to understand the dynamical changes of bio-optical properties, primary productivity, and carbon fluxes of the upper ocean on time scales ranging from minutes to decades. In particular, use of biweekly subsampled data (e.g., as sampled by *Menzel and Ryther* [1960, 1961] and others restricted to shipboard measurements) for determinations of biomass, primary production, and carbon export would result in significant underestimates for most of the observational period described here [*Dickey*, 1991]. Fortunately, technical advances have made it possible to sample several of the key variables virtually continuously.

Observations of bio-optical and physical phenomena from moorings, ships, and satellites all have sampling advantages and disadvantages [e.g., *Dickey*, 1991]. Moored observations in conjunction with shipboard measurements and remotely sensed data will continue to be cornerstones of process-oriented studies. Moored observations can be used to "ground truth" as well as complement remote sensing observations of ocean color, temperature, and other properties. For example, moored bio-optical and physical measurements can be used to (1) provide near-surface and subsurface (e.g., depths greater than an optical attenuation depth) data for the development of algorithms for satellite sensing of ocean color and the inference of pigment biomass and primary productivity, (2) complement satellite data sets which are lower in sampling frequency, subject to sampling biases (e.g., cloud conditions), and limited to near-surface integrated measurements (thus undersampling chlorophyll maxima), (3) provide data between satellite missions, and (4) facilitate the development of coupled physical and bio-optical models [also see *Smith et al.*, this issue; *Dickey*, 1991]. Ultimately, the long-term monitoring and model prediction of changes in bio-optical properties and particulate carbon fluxes will benefit from the synthesis of data derived from a suite of complementary observational platforms [e.g., *Dickey*, 1991].

Acknowledgments. This research was sponsored by the Office of Naval Research as part of the Biowatt program (contracts N00014-87-K0084 (TD) and N00014-86-K0204 (JM)). We wish to acknowledge the technical assistance provided by Derek Manov, Miguel Maccio, John Scott, Ivars Bitte, and Larry Sullivan. We would also like to express our appreciation to Eric Hartwig, Burt Jones, Ray Smith, Libe Washburn, and Kirk Waters for their comments and suggestions.

REFERENCES

Ackleson, S. G., J. J. Cullen, J. Brown, and M. P. Lesser, Some changes in the optical properties of marine phytoplankton in response to high light intensity, *Ocean Opt., 10*, 238 - 249, 1990.

Bartz, R., J. R. V. Zaneveld, and H. Pak, A transmissometer for profiling and moored observations in water, *Ocean Opt., 5*, 102 - 108, 1978.

Bartz, R., R. Spinrad, and J. C. Kitchen, A low power, high resolution, in situ fluorometer for profiling and moored applications in water, *Ocean Opt., 9*, 157 - 170, 1988.

Bidigare, R. R., J. Marra, T. D. Dickey, R. Iturriaga, H. Pak, and R. C. Smith, Evidence for phytoplankton succession and chromatic adaptation in the Sargasso Sea during springtime 1985, *Mar. Ecol. Prog. Ser., 60*, 113 - 122, 1989.

Bishop, J. K. B., The correction and suspended matter calibration of Sea Tech transmissometer data, *Deep Sea Res., 33,* 121 - 134, 1986.

Booth, C. R., The design and evaluation of a measurement system for photosynthetically active quantum scalar irradiance, *Limnol. Oceanogr., 19,* 326 - 335, 1976.

Booth, C.R., and R. C. Smith, Moored spectroradiometers in the Biowatt experiment, *Ocean Opt., 9,* 176 - 188, 1988.

Booth, C. R., B. G. Mitchell, and O. Holm-Hansen, Development of moored oceanographic spectroradiometer, *Biospherical Tech. Ref. 87-1,* Biospherical Instrum., Inc., San Diego, Calif., 1987.

Brewer, P. G., K. W. Bruland, R. W. Eppley, and J. J. McCarthy, The Global Ocean Flux Study (GOFS): Status of the U.S. GOFS Program, *Eos, Trans. AGU, 67,* 827 - 832, 835 - 837, 1986.

Briscoe, M. G., and R. A. Weller, Preliminary results from the Long-Term Upper-Ocean Study (LOTUS), *Dyn. Atmos. Oceans, 8,* 243 - 265, 1984.

Brown, O. B., R. H. Evans, J. W. Brown, H. R. Gordon, R. C. Smith, and K. S. Baker, Phytoplankton blooming off the U.S. east coast: A satellite description, *Science, 229,* 163 - 167, 1985.

Bunker, A. F., Energy exchange at the surface of the western North Atlantic Ocean, *Tech. Rep., WHOI-75-3,* Woods Hole Oceanogr. Inst., Woods Hole, Mass., 1975.

Bunker, A. F., Computations of surface energy flux and annual air-sea interaction cycles of the North Atlantic Ocean, *Mon. Weather Rev., 104,* 1122 - 1140, 1976.

Chai, Z., T. Dickey, J. Vazquez, and J. Wiggert, Observations of mesoscale features in the Sargasso Sea in 1987 using satellite, ship-based, and mooring measurements, *Tech. Rep., OPG-91-01,* 160pp., Univ. of Southern California, Los Angeles, Calif., 1991.

Cornillon, P., D. Evans, and W. Large, Warm outbreaks of the Gulf Stream into the Sargasso Sea, *J. Geophys. Res., 91,* 6583 - 6596, 1986.

Cullen, J. J., E. Stewart, E. Renger, R. W. Eppley, and C. D. Winant, Vertical motion of the thermocline, nutricline, and chlorophyll maximum layers in relation to currents on the southern California shelf, *J. Mar. Res., 41,* 239 - 262, 1983.

Dean, J. P., and R. C. Beardsley, A Vector-Averaging Wind Recorder (VAWR) system for surface meteorological measurements in CODE (Coastal Ocean Dynamics Experiment), *Tech. Rep. WHOI Ref. 88 - 20,* 74 pp., Woods Hole Oceanogr. Inst., Woods Hole, Mass., 1988.

Deser, C., R. A. Weller, and M. G. Briscoe, Long-Term Upper-Ocean Study (LOTUS) at 34°N, 70°W: Meteorological sensors, data, and heat fluxes for May - October 1982 (LOTUS-3 and LOTUS-4), *Tech. Rep., WHOI-83-22,* 68 pp., Woods Hole Oceanogr. Inst., Woods Hole, Mass., 1983.

Dickey, T. D., Recent advances and future directions in multi-disciplinary in situ oceanographic measurement systems, in *Toward a Theory on Biological and Physical Interactions in the World Ocean,* edited by B. J. Rothschild, pp. 555 - 598, Kluwer Academic, Dordrecht, Netherlands, 1988.

Dickey, T.D., Physical-optical-biological scales relevant to recruitment in large marine ecosystems, in *Large Marine Ecosystems: Patterns, Processes, and Yields,* edited by K. Sherman, L. M. Alexander, and B. D. Gold, pp. 82 - 98, AAAS, Washington, D. C., 1990.

Dickey, T., The emergence of concurrent high resolution physical and bio-optical measurements in the upper ocean and their applications, *Rev. Geophys.,* in press, 1991.

Dickey, T. D., E. O. Hartwig, and J. Marra, The Biowatt bio-optical and physical moored measurement program, *Eos, 67,* 650, 1986*a*.

Dickey, T., D. A. Siegel, A. Bratkovich, and L. Washburn, Optical features associated with thermohaline structures, *Ocean Opt., 8,* 308 - 313, 1986*b*.

Dickey, T. D., D. A. Siegel, S. Boztas, and M. K. Hamilton, Biowatt I multi-variable profiler (MVP), technical report, Ocean Phys. Group, Univ. of Southern Calif., Los Angeles, 1986*c*.

Dickey, T., T. Granata, M. Hamilton, J. Wiggert, D. Manov, D. Siegel, Z. Chai, M. Stramska, and J. Scott, Final report on the multi-variable moored system (MVMS) and meteorological data sets collected during the Biowatt II experiment in the Sargasso Sea in 1987, *Tech. Rep., OPG-90-01,* 215 pp., Univ. of Southern Calif., Los Angeles, Calif., 1990*a*.

Dickey, T., T. Granata, M. Hamilton, J. Wiggert, J. Marra, C. Langdon, and D. A. Siegel, Time series observations of bio-optical properties in the upper layer of the Sargasso Sea, *Ocean Opt., 10,* 202 - 214, 1990*b*.

Emerson, S., Seasonal oxygen cycles and biological new production in surface waters of the subarctic Pacific Ocean, *J. Geophys. Res., 92,* 6535 - 6544, 1987.

Eppley, R. W., and B. W. Peterson, Particulate organic matter flux and planktonic new production in the deep ocean, *Nature, 282,* 677 - 680, 1979.

Eriksen, C. C., Variability in the upper-ocean internal wave field at a Sargasso Sea site, *J. Phys. Oceanogr., 18,* 1495 -1513, 1988.

Falkowski, P. G., C. N. Flagg, G. T. Rowe, S. L. Smith, T. E. Whitledge, and C. D. Wirick, The fate of the spring phytoplankton bloom: Export or oxidation, *Cont. Shelf Res., 8,* 457 - 484, 1988.

Fukuchi, M., H. Hattori, H. Sasaki, and T. Hoshiai, A phytoplankton bloom and associated processes observed with a long-term moored system in Antarctic waters, *Mar. Ecol. Prog. Ser., 45,* 279 - 288, 1988.

Fukuchi, M., K. Watanabe, A. Tanimura, T. Hoshiai, H. Sasaki, H. Satoh, and Y. Yamaguchi, A phytoplankton bloom under sea ice recorded with a moored system in lagoon Saroma Ko, Hokkaido, Japan, *Proc. NIPR Symp. Polar Biol., 2,* 9 - 15, 1989.

Garrett, C., and W. Munk, Space-time scales of internal waves, *Geophys. Fluid Dyn., 2,* 225 - 264, 1972.

Gonella, J., A rotary-component method for analyzing meteorological and oceanographic vector time series, *Deep Sea Res., 19,* 833 - 846, 1972.

Gordon, H. R., and A. Y. Morel, *Remote Assessment of Ocean Color for Interpretation of Satellite Visible Imagery, A Review, Lect. Notes Coastal Estuarine Stud.,* 114 pp., Springer-Verlag, New York, 1983.

Gordon, H. R., O. B. Brown, R. H. Evans, J. W. Brown, R, C. Smith, K. S. Baker, and D. K. Clark, A semi-analytic radiance model of ocean color, *J. Geophys. Res., 93,* 10,909 - 10,924, 1988.

Hamilton, T. Granata, T. Dickey, J. Wiggert, D. Siegel, J. Marra, and C. Langdon, Diurnal variations of bio-optical properties in the Sargasso Sea, *Ocean Opt., 10,* 214 - 224, 1990.

Hellerman, S., and M. Rosenstein, Normal monthly wind stress over the world ocean with error estimates, *J. Phys. Oceanogr., 13,* 1093 - 1104, 1983.

Jenkins, W. J., and J. C. Goldman, Seasonal oxygen cycling and primary production in the Sargasso Sea, *J. Mar. Res., 43,* 465 - 491, 1985.

Kiefer, D. A., Chlorophyll *a* fluorescence in marine centric diatoms: Responses of chloroplasts to light and nutrient stress, *Mar. Biol., 23,* 39 - 46, 1973.

Kiefer, D. A., and B. G. Mitchell, A simple, steady-state description of phytoplankton growth based on absorption cross section and quantum efficiency, *Limnol. Oceanogr., 28,* 770 - 776, 1983.

Kiefer, D. A., W. S. Chamberlain, and C. R. Booth, Natural fluorescence of chlorophyll *a*: Relationship to photosynthesis and chlorophyll concentration in the western South Pacific gyre, *Limnol. Oceanogr., 34,* 868 - 881, 1989.

Kondo, J., Air-sea bulk transfer coefficients in diabatic conditions, *Boundary Layer Meteorol., 9,* 91 - 112, 1975.

Kunze, E., Near-inertial wave propagation in geostrophic shear, *J. Phys. Oceanogr.*, *15*, 544 - 565, 1985.

Langdon, C., Dissolved oxygen monitoring system using a pulsed electrode: Design, performance, and evaluation, *Deep Sea Res.*, *31*, 1357 - 1367, 1984.

Liu, W. T., K. B. Katsaros, and J. Businger, Bulk parameterizations of air-sea exchanges of heat and water vapor including molecular constraints at the interface, *J. Atmos. Sci.*, *36*, 1722 - 1735, 1979.

Liu, W. T., T. V. Blanc, T. Liu, K. Katsaros, and J. Businger, Bulk atmospheric flux computational iteration program in FORTRAN and BASIC, *Memor. Rep. 5291*, Nav. Res. Lab., Washington, D. C., 1984.

Marra, J., R., R. Bidigare, T. D. Dickey, Nutrients and mixing, chlorophyll and phytoplankton growth, *Deep Sea Res.*, *37*, 127 - 143,1990.

Menzel, D. W., and J. H. Ryther, The annual cycle of primary production in the Sargasso Sea off Bermuda, *Deep Sea Res.*, *6*, 351 - 367, 1960.

Menzel, D. W. and J. H. Ryther, Annual variations in primary production of the Sargasso Sea off Bermuda, *Deep Sea Res.*, *7*, 282 - 288, 1961.

Michaelsen, J., X. Zhang, and R. C. Smith, Variability of pigment biomass in the California Current as determined by satellite imagery, 2: Temporal variability, *J. Geophys. Res.*, *93*, 10,883 - 10,896, 1988.

Mooers, C. N. K., Several effects of a baroclinic current on the cross-stream propagation of inertial-internal waves, *J. Phys. Oceanogr.*, *6*, 245 - 275, 1975*a*.

Mooers, C. N. K., Several effects of a baroclinic current on the three-dimensional propagation of inertial-internal waves, *J. Phys. Oceanogr.*, *6*, 277 - 284, 1975*b*.

Musgrave, D. L., J. Chou, and W. J. Jenkins, Application of a model of upper ocean physics for studying seasonal cycles, *J. Geophys. Res.*, *93*, 15,679 - 15,700, 1988.

Platt, T., W. G. Harrison, M. L. Lewis, W. K. W. Li, S. Sathyendranath, R. E. Smith, and A.F. Vezina, Biological production of the oceans: The case for a consensus, *Mar. Ecol. Prog. Ser.*, *52*, 77 - 88, 1989.

Powell, T. M., P. J. Richerson, T. M. Dillon, B. A. Agee, B. J. Dozier, D. A. Godden, and L. O. Myrup, Spatial scales of current speed and phytoplankton biomass fluctuations in Lake Tahoe, *Science*, *189*, 1088 - 1089, 1975.

Richardson, P. L., Eddy kinetic energy in the North Atlantic from surface drifters, *J. Geophys. Res.*, *88*, 4355 - 4367, 1983.

Siegel, D. A., and T. D. Dickey, On the parameterization of irradiance for ocean photoprocesses, *J. Geophys. Res.*, *92*, 14,648 - 14,662, 1987.

Siegel, D. A., T. D. Dickey, L. Washburn, M. K. Hamilton, and B. G. Mitchell, Optical determination of particulate abundance and production variations in the oligotrophic ocean, *Deep Sea Res.*, *36*, 211 - 222, 1989.

Siegel, D. A., R. Iturriaga, R. R. Bidigare, R. C. Smith, H. Pak, T. D. Dickey, J. Marra, and K. S. Baker, Meridional variations of the springtime phytoplankton community in the Sargasso Sea, *J. Mar. Res.*, *48*, 379 - 412, 1990.

Smith, R. C., O. B. Brown, F. E. Hoge, K. S. Baker, R. H. Evans, R. N. Swift, and W. E. Esaias, Multiplatform sampling (ship, aircraft, and satellite) of a Gulf Stream warm core ring, *Appl. Opt.*, *26*, 2068 - 2081, 1987*a*.

Smith, R. C., R. R. Bidigare, B. B. Prezlin, K. S. Baker, and J. M. Brooks, Optical characterization of primary production across a coastal front, *Mar. Biol.*, *96*, 575 - 591, 1987*b*.

Smith, R. C., K. J. Waters, and K. S. Baker, Optical variability and pigment biomass in the Sargasso Sea as determined using deep-sea optical mooring data, *J. Geophys. Res.*, this issue.

Spinrad, R. W., A calibration diagram of specific beam attenuation, *J. Geophys. Res.*, *91*, 7761 - 7764, 1986.

Spinrad, R. W., Testing of optical properties and development of application procedure for OMP-8 antifoulant on submersible optical surfaces, *Ref. Tech. Rep. 8701*, 44 pp., *Sea Tech, Inc., Corvallis, Ore.*, 1987.

Sverdrup, H. U., On the conditions for vernal blooming of phytoplankton, *J. Cons. Perm. int. Explor. Mer*, *18*, 287-295, 1953.

Swift, E., J. Van Keuren, H. P. Batchelder, C. R. Booth, and C. P. Li, Moored instrument to measure stimulated and natural oceanic bioluminescence, *Ocean Opt.*, *9*, 75 - 86, 1988.

Thomson, R. E., T. A. Curran, M. C. Hamilton, and R. McFarlane, Time series measurements from a moored fluorescence-based dissolved oxygen sensor, *J. Atmos. Ocean. Technol.*, *5*, 614 - 624, 1988.

Washburn, L., D. A. Siegel, T. D. Dickey, and M. K. Hamilton, Isopycnal mixing and the distribution of particles across the North Pacific Subtropical Front, *Deep Sea Res.*, *36*, 1607 - 1620, 1989.

Weller, R. A., The relation of near-inertial motions observed in the mixed layer during the JASIN (1978) experiment to the local wind stress and to the quasi-geostrophic flow field, *J. Phys. Oceanogr.*, *12*, 1122 - 1136, 1982.

Weller, R., and R. E. Davis, A vector measuring current meter, *Deep Sea Res.*, *27*, 565 - 582, 1980.

Weller, R. A., and D. Halpern, The velocity structure of the upper ocean in the presence of surface forcing and mesoscale eddies, *Philos. Trans. R. Soc. London, Ser. A*, *308*, 327 - 340, 1983.

Weller, R. A., D. L. Rudnick, R. E. Payne, J. P. Dean, N. J. Pennington, and R. P. Trask, Measuring near-surface meteorology over the ocean from an array of surface moorings in the Subtropical Convergence Zone, *J. Atmos. Oceanic Technol.*, *7*, 85 - 103, 1990.

Welschmeyer, N. A., and C. J. Lorenzen, Chlorophyll budgets: Zooplankton grazing and phytoplankton growth in a temperate fjord and the central Pacific Ocean, *Limnol. Oceanogr.*, *30*, 1 - 21, 1986.

Whitledge, T. E., and C. D. Wirick, Observations of chlorophyll concentrations off Long Island from a moored in situ fluorometer, *Deep Sea Res.*, *30*, 297 - 309, 1983.

Whitledge, T. E., and C. D. Wirick, Development of a moored in situ fluorometer for phytoplankton studies, in *Tidal Mixing and Plankton Dynamics*, Lect. Notes Coastal Estuarine Stud., vol. 17, edited by M. J. Bowman, C. M. Yentsch, and W. T. Peterson, pp. 449 - 462, Springer-Verlag, Berlin, 1986.

Worthington, L.V., The 18° water in the Sargasso Sea, *Deep Sea Res.*, *5*, 297 - 305, 1959.

A. Bratkovich, NOAA Great Lakes Environmental Research Laboratory, and Department of Atmospheric, Oceanic, and Space Sciences, University of Michigan, 2205 Commonwealth Blvd., Ann Arbor, MI 48105.

T. Dickey, T. Granata, M. Hamilton, and J. Wiggert, Ocean Physics Group, Department of Geological Sciences, University of Southern California, Los Angeles, CA 90089-0740.

C. Langdon and J. Marra, Lamont-Doherty Geological Observatory, Palisades, NY 10964.

D. Siegel, Department of Geography, University of California, Santa Barbara, CA 93106.

(Received June 12, 1990;
accepted August 22, 1990.)